JPCBFK

VOLUME 108
MARCH 18, 2004
NUMBER 11
http://pubs.acs.org/JPCB

THE JOURNAL OF PHYSICAL CHEMISTRY B

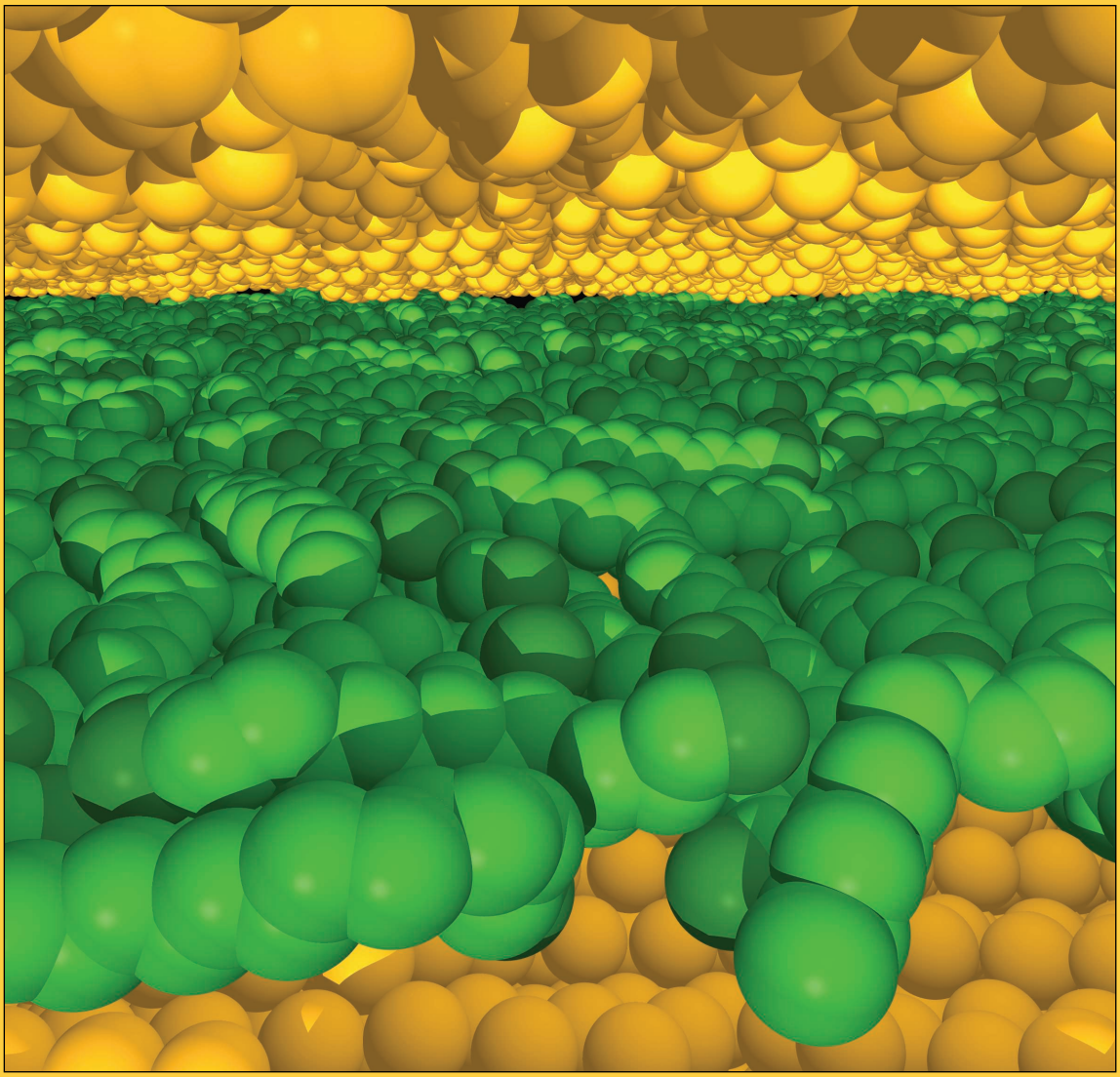

Simulated Hexadecane Molecules Confined by Atomically Rough Gold Surfaces Exhibiting Amontons' Friction Law
(see page XXX)

CONDENSED MATTER, MATERIALS, SURFACES, INTERFACES, & BIOPHYSICAL CHEMISTRY

PUBLISHED WEEKLY BY THE AMERICAN CHEMICAL SOCIETY

11 | 108 MARCH 18, 2004 VOL. 108 NO. 11 The Journal of Physical Chemistry B PP. XXXXX–XXXXX

Frictional Forces and Amontons' Law: From the Molecular to the Macroscopic Scale

Jianping Gao,[†] W. D. Luedtke,[†] D. Gourdon,[‡] M. Ruths,[§] J. N. Israelachvili,[‡] and Uzi Landman*,[†]

School of Physics, Georgia Institute of Technology, Atlanta, Georgia 30332-0430, Department of Chemical Engineering, University of California, Santa Barbara, California 93106, and Department of Physical Chemistry, Åbo Akademi University, Porthansgatan 3-5, FIN-20500 Åbo, Finland

Received: August 8, 2003; In Final Form: December 9, 2003

We review the historical and modern understanding of the most basic equation of friction, Amontons' law, which describes phenomena that were already understood and studied by Leonardo da Vinci 500 years ago. This law states that for any two materials the (lateral) friction force is directly proportional to the (normal) applied load, with a constant of proportionality, the friction coefficient, that is constant and independent of the contact area, the surface roughness, and the sliding velocity. No theory has yet satisfactorily explained this surprisingly general law; all attempts have been model or system dependent. We review the experimental evidence and find, for example, that the same friction coefficient is often measured for the same system of materials with junctions whose areas differ by more than 6 orders of magnitude. The trends obtained through molecular dynamics (MD) simulations agree with recent and past experiments and with Amontons' law, and they suggest that the local energy-dissipating mechanisms are not merely "mechanical", as assumed in most models, but "thermodynamic" in nature, like miniature irreversible compression−decompression cycles of the trapped molecules between the surface asperities as they pass over each other. The MD analysis reveals that, for such dynamic, nonequilibrium, energy-dissipating processes, a proper statistical description can be formulated through the use of the Weibull distribution of the local friction forces, which may be regarded to serve in this context a similar purpose as the Boltzmann distribution for classical systems at equilibrium. Another important conclusion is that the concept of the "real" area of contact is a nonfundamental quantity, whether at the nano-, micro-, or macroscale. However, it may serve as a convenient scaling parameter for describing the really fundamental parameters, which are the number density of atoms, molecules, or bonds involved in an adhesive or frictional interaction.

1. Brief History of the Concept of the "Coefficient of Friction"

The coefficient of friction (COF), or friction coefficient, is a constant defined by

$$\mu = \frac{\text{lateral (friction) force}}{\text{normal (externally applied) load}} = \frac{F}{L} \qquad (1a)$$

or

$$\mu' = \frac{\mathrm{d}F}{\mathrm{d}L} \qquad (1b)$$

In the first definition, $F = 0$ at $L = 0$; i.e., the friction force is zero at zero load, while in the second definition, the friction force may be finite at zero load and the COF is given by the slope of the line. Friction coefficients are tabulated in manuals and handbooks, are used in the design of machinery as well as in the construction industry,[1] and play a key role in many lawsuits. And yet this quantity is not a constant; that is, it is material dependent, and it is often found to take different values for different conditions (e.g., humidity, smooth or rough morphologies) of the sliding surfaces. Moreover, there are many instances where the above equations, especially eq 1a, do not apply at all, for example, in situations where there is friction even at zero or negative loads.

Early Phenomenological Observations and Theories of Friction. A "friction" force is different from a conventional applied force which in the Newtonian definition acts on a body from the outside and causes it to accelerate. The friction force is not an independent external force that acts on a body but an internal force that opposes the externally applied force. Thus, it may be thought of as a *reaction* force rather than an *action* force. In this sense, it is similar to the adhesion force between two bodies, which appears only when one tries to separate the bodies from contact.[2] Bearing this difference in mind is important both in practice and in theoretical modeling of friction (and adhesion).

The first recorded systematic studies of friction were made by Leonardo da Vinci (1452−1519). He measured the friction

* Author to whom correspondence should be addressed. E-mail: uzi.landman@physics.gatech.edu.
[†] Georgia Institute of Technology.
[‡] University of California, Santa Barbara.
[§] Åbo Akademi University.

10.1021/jp036362l CCC: $27.50
Published on Web 00/00/0000 PAGE EST: 15.1

force F needed to slide a mass M (equivalent to an external compressive load L) across a surface, most probably wood on wood and wood on iron combinations,[3] and made two important observations: first, he concluded that the friction force doubled when the weight was doubled (i.e., that F was proportional to L); and second, he concluded that the friction force was independent of the way the objects were positioned on the surface (i.e., that F did not depend on the area of contact A between the moving surfaces). These observations were later confirmed by Amontons (1663−1706),[4] and Coulomb further noted the velocity independence of the friction force.[3] These three observations can be summarized as follows

$$\mu = F/L = \text{constant (independent of } A \text{ and } V) \qquad (2)$$

where A and V are the ("apparent" or macroscopic) contact area and sliding velocity, respectively. While we now know that eq 2 is not valid over large ranges of loads and/or sliding velocities[5,6] and that it completely breaks down for atomically smooth surfaces in strongly adhesive contact,[7] it remains surprisingly good at describing the majority of rubbing surfaces involving both dry and lubricated contacts, both ductile and brittle, both rough and smooth surfaces (so long as they are not adhesive), and both macroscopic and microscopic contacts.[8,9] For 500 years, until the recent development of sophisticated computer simulations of dynamic many-body systems, this apparently quite general equation defied a satisfactory model-independent explanation, which is the subject of this article.

All the terms in Amontons' law refer to macroscopic, i.e., space- and time-averaged or "mean-field", values. Thus, the contact area is the "apparent" or projected geometric area rather than the "real" contact area at the molecular level. And V is the mean relative velocity of the sliding bodies even though the shearing microjunctions may be moving with large fluctuations or in a stick-slip fashion.[10] Early attempts to account for Amontons' law, first by Amontons[4] and later by Coulomb (1736−1806)[11] and Euler (1707−1783),[12] were based on analyses of how the microscopic surface asperities of one surface would have to climb over those of the other to allow for two surfaces to slide past each other. The argument went something like this: Since the lateral local friction force F needed to lift an asperity equals the normal (local) load L multiplied by tan θ, where θ is the maximum slope of the asperity junction, we immediately obtain $F_i/L_i = \tan \theta_i$ at the ith asperity. When averaged over all asperities, it was reasonable to expect the space-averaged angle θ and therefore tan θ to be constant, viz., $\langle \tan \theta_i \rangle = \text{constant}$. Denoting the total friction force by F, we may write

$$F = \sum F_i = \sum L_i \tan \theta_i = \langle \tan \theta_i \rangle L = \mu L \qquad (3)$$

where L is the total load, and in the third equality we assumed that on average the local values of tan θ_i and L_i are uncorrelated. In the above, μ is the macroscopic friction coefficient, which is also seen to be independent of the contact area A or velocity V (since neither of these parameters ever enter into the picture). And since adhesion is never considered, the model implicitly applies only to nonadhering surfaces.

Various arguments, both experimental and theoretical, were soon raised against this purely geometrical and mechanistic interpretation of friction notably by Leslie[13] in 1804 who argued that the energy expended on dragging an asperity to the top of another is simply recovered when it falls down on the other side. Thus, no energy is ever lost; the two surfaces should simply continue to move once they are set in motion without the need of a constant driving force (to overcome the nonexistent friction force). Some other "energy-dissipating" mechanism was therefore called for. In a series of classic experiments, Bowden and Tabor[14,15] found that the electrical conductivity at a metal−metal interface was proportional to the load pressing the two (rough) surfaces together and thereby concluded that the "real" area of contact is proportional to the load ($A \propto L$). Since the lateral force needed to shear or plastically deform a junction is also proportional to the area of the junction, they immediately arrived at Amontons' law.

But the Bowden−Tabor (BT) theory was inconsistent with the Hertz theory[16] of nonadhering elastic junctions, which predicts that $A \propto (RL)^{2/3}$ for a sphere of radius R on a flat surface. Furthermore Maugis and Pollock[17] investigated, in the context of metal microcontacts, the development of full plastic deformation of junctions and predicted $A \propto R^{1/2}L$. Some reconciliation was achieved by Greenwood and Williamson (GW),[18,19] who showed that, for two rough (nonadhering) surfaces having an exponential distribution of asperity heights (all asperities were assumed to have spherical caps of equal radius), the real contact area would indeed be proportional to the applied load if the asperities deformed elastically. Other assumptions, or limitations, of the GW theory include the application of the macroscopic (continuum) Hertzian theory of elastic deformations to microscopic and nanoscopic asperities, the assumption of identical asperity radii, and the inability to extend it to atomic or molecular-scale structures, as well as the very important fundamental assumption concerning the area dependence of the "shear strength". All this makes the GW theory highly model dependent, especially if one wants to apply it more widely, e.g., to lubricated, plastically deforming, or molecular-scale systems. The GW approach motivated certain extensions of the original work, as well as generalizations of the statistical model approach to the treatment of other models of contact (incorporating effects of plasticity and wear,[20] adhesion,[21,22] and fractal geometries).[23,24] Nevertheless, in light of their assumptions, it is doubtful that both the BT and GW theories could account for all the cases where eq 1 has been found to hold as, for example, in situations involving wearless sliding, and it is timely to explore other approaches for the elucidation of the origins of Amontons' law. In this context, we call attention to a self-assessment by Greenwood of certain key aspects of the GW theory titled "Surface Roughness and Contact: An Apology".[25]

For adhering surfaces, Derjaguin[26] proposed the following modified version of Amontons' equation

$$F = \mu(L_0 + L) = F_0 + \mu L \qquad (4)$$

where a constant "internal" load L_0 is added to the external load L to account for the intermolecular adhesive forces.[27] The Derjaguin equation accounted for the experimental observation that there is already a finite friction force F_0 at zero load for adhering surfaces, but this equation is even more difficult to reconcile with the Johnson−Kendall−Roberts[28] (JKR) theory of adhering junctions. In addition, the friction coefficient is not constant when it is defined from eq 4 as the ratio $F/L = \mu(1 + L_0/L)$, which gives $\mu = \infty$ at zero load, but it is constant when defined as the slope, $dF/dL = \mu = \text{constant}$, which is the common convention in such cases.

2. Recent Experimental and Theoretical Insights

With the advent of the atomic force microscope[29] (AFM) and the surface forces apparatus[30,31,32] (SFA), it has become possible

to explore and elucidate on the molecular level the physical mechanisms and energy-conversion processes operating at real sliding contacts. The AFM and SFA have proved to be ideal tools for nano-, micro-, and macroscopic tribological experiments[33−38] for measuring both normal and lateral forces between (i) a nanometer-radius tip and a sample surface, (ii) a micrometer-sized colloidal probe and a sample surface, and (iii) two extended molecularly smooth surfaces that confine between them a lubricant film of known (measurable) thickness and real contact area. Both wear and wearless friction can be studied on extended surfaces or model single-asperity junctions. These experimental advances have enabled the testing of existing theories of continuum contact mechanics, the Hertz[16] and JKR[28] theories for nonadhering and adhering contacts, and of establishing relationships between adhesion and friction. Such experiments have also been correlated with recent theoretical advances where continuum and mean-field theories have become replaced by atomistic models, usually involving molecular dynamics (MD) computer simulations.[33,39−45]

In this paper, we first review and present some new results on experimental friction data obtained with the SFA and AFM techniques on a variety of adhering and nonadhering surfaces, both dry and lubricated, soft and hard, and smooth and rough. We then present new large-scale MD simulations of two solid rough (as well as smooth) shearing surfaces with a thin hydrocarbon liquid film confined between them. The experimental aim was to test the range of applicability of Amontons' law for widely different systems and length scales, while the theoretical aim was to establish the reason for its widespread applicability and to explore whether it holds both at the macroscopic and local (nanoscopic) levels. We find that the trends observed in the experiments and obtained through the theoretical simulations are consistent with each other, although different materials and conditions were employed in the two methods of investigations. Interestingly, in the simulations, we do not find a linear relationship between the friction force and the normal load at the local level but do find a linear relationship between F and L (i.e., Amontons' law) for the time- and space-averaged quantities. In addition, the concept of a contact area, whether "real" or "apparent", never enters into the picture or any fundamental equation (e.g., in describing the energy exchange between colliding molecules), although it may serve as a convenient scaling parameter for describing the fundamental parameters, which are the number density of atoms, molecules, or bonds involved in an adhesive or frictional interaction.

Recent Experiments. In this section, we present experimental friction data obtained with the SFA and the friction force microscope[46] (FFM) on a variety of adhesive and nonadhesive systems. We also make comparisons with tribological measurements made on macroscopic surfaces using conventional pin-on-disk tribometers. Both the SFA and the FFM can measure the friction forces at single-asperity contacts, but there is a large difference in the contact areas and pressures obtained with these two techniques; the radius of curvature of the undeformed surfaces in an SFA experiment is typically $R = 0.2-2$ cm, whereas FFM tips typically have radii of $R = 10-300$ nm, or $R = 1-10$ μm if a colloidal bead is attached to the end of the cantilever spring. Within the load range that can be conveniently reached in the SFA, the *maximum* pressure in the contact area is usually less than 0.1 GPa, whereas typical contact pressures in FFM experiments, even at low loads, are already several GPa.[47] Still, as we shall see, when comparing the sliding of different (low-adhesion) single-asperity contacts with each other, and with the sliding of rough or damaged surfaces having many

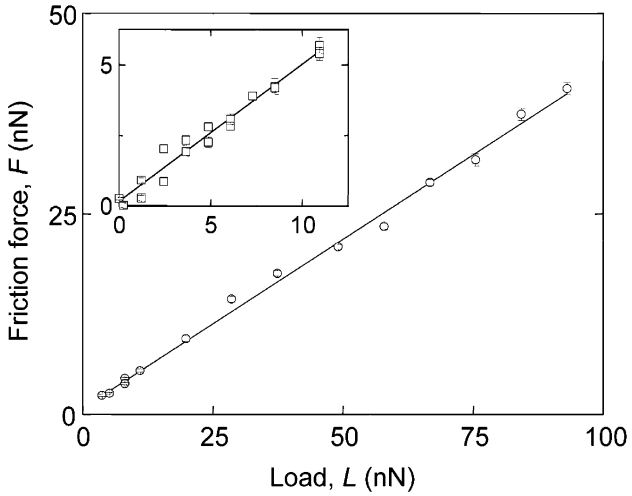

Figure 1. FFM measurements in ethanol of the friction force F between bare template-stripped gold surfaces and two unfunctionalized Si tips of different radii and spring constants. Main figure: $R = 33$ nm, $\mu = 0.42 \pm 0.01$. Inset: $R = 11$ nm, $\mu = 0.49 \pm 0.02$. Sliding velocity: $V = 0.15$ μm/s. Adapted from Ruths, M. *Langmuir* **2003**, *19*, 6788. Copyright 2003 American Chemical Society.

contacts, one often finds a linear dependence of F on L, sometimes even with the same friction coefficient.[48] We start by concentrating on the friction of nonadhering surfaces, for which eqs 1 and 2 were developed.[49] Since it is difficult to avoid adhesion in air, especially between atomically smooth surfaces, these were immersed in a liquid such as ethanol (cf. Figures 1 and 2), which significantly reduced the adhesion forces between the surfaces due to the reduced van der Waals force (reduced Hamaker constant) and/or oscillatory structural force between the surfaces in liquids.[50]

Figure 1 shows the friction force as a function of applied load of unmodified silicon FFM tips (with a native oxide layer) sliding on gold surfaces in ethanol.[51] The measured interfacial energy for this system was $\gamma < 2$ mJ/m^2, which is low when compared to values of order $\gamma = 20-30$ mJ/m^2 for van der Waals solids (e.g., surfactant monolayers) in air and $\gamma > 1000$ mJ/m^2 for metallic contacts. In the load range investigated, the gold surfaces were not damaged during sliding, and despite a difference in tip radii by a factor of 3, F increased linearly with L, passing through the origin at low loads, and with a similar slope (friction coefficient) for both tips. By assumption of a Hertzian contact for these nonadhesive junctions, the contact area would vary as $A \propto (RL)^{2/3}$, and if the friction were to scale with the area as occurs for *adhesive* contacts,[37,52−54] (cf. Figure 7), the data points in Figure 1 would not fall on a straight line. Apparently, the chosen condition of low adhesion reduces the area-dependence of the friction, at least for this range of tip radii and loads, and one obtains a purely load-dependent friction force, i.e., Amontons' equation.

Figure 2 shows the friction force measured with both SFA and FFM on a system where both sliding surfaces were covered with a chemically bound benzyltrichlorosilane monolayer (molecular area 0.27 nm^2).[55] As in the case of Si against gold in ethanol (Figure 1), very different contact areas and loads still give a linear dependence of F on L with the same friction coefficient for comparable systems, and again $F \rightarrow 0$ as $L \rightarrow 0$. In the FFM measurements (Figure 2b), the plateau in the data at higher loads suggests a transition in the monolayers, similar to previous observations on alkanethiol[56,57] and aromatic thiol monolayers on gold.[51] The pressure in the contact region in the SFA is much lower than in the FFM, and no transitions in the

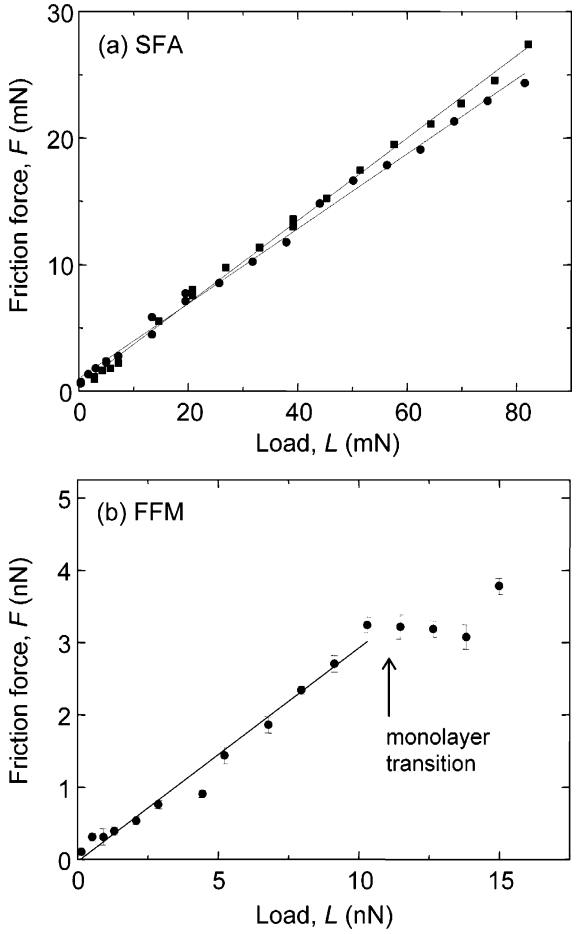

Figure 2. Friction force between benzyltrichlorosilane monolayers chemically bound to glass or Si in ethanol (γ < 1 mJ/m^2). (a) SFA measurements where both glass surfaces were covered with a monolayer. Circles and squares show two different experiments: one with R = 2.6 cm, V = 0.15 μm/s, giving μ = 0.33 ± 0.01; the other with R = 1.6 cm, V = 0.5 μm/s, giving μ = 0.30 ± 0.01. (b) FFM measurements of the same monolayer-functionalized Si tip (R = 11 nm) sliding on a monolayer-covered glass surface at V = 0.15 μm/s, giving μ = 0.30 ± 0.01. Adapted from Ruths, M.; Alcantar, N. A.; Israelachvili, J. N. *J. Phys. Chem.* **2003**, *107*, 11149. Copyright 2003 American Chemical Society.

friction forces or in the thicknesses of the confined layers where observed in the SFA experiments (and no damage to the monolayers or the underlying substrates was observed during the experiments, indicating that the friction was "wearless").

Despite the more than 6 orders of magnitude difference in the contact radii, pressure, loads, and friction forces, the measured friction coefficients obtained with the two techniques for these similar systems are practically the same. A recent study of the friction between two covalently bound aromatic thiol monolayers under conditions of low adhesion (γ = 1−4 mJ/m^2) showed a similar agreement for the friction coefficients obtained with FFM tips of very different radii.[51] Evidently, this conclusion can be extended to experiments with the SFA where R is 5−6 orders of magnitude larger.[58]

A linear increase in the friction force with load can also be observed in systems that become damaged during sliding. Figure 3 shows the results of SFA experiments in dry and humid air using an industrially important surface, alumina (aluminum oxide, prepared by e-beam evaporation of Al_2O_3 onto mica substrates to form a smooth 10-nm-thick film).[59] Both untreated and surfactant-coated surfaces were studied.[60] In the case of smooth surfaces (curves a and c), there is adhesion and the

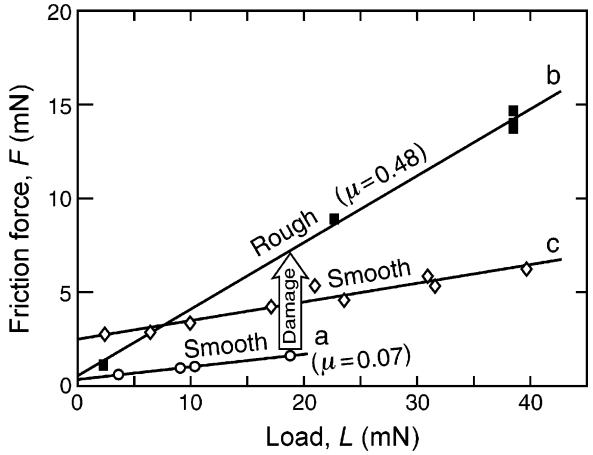

Figure 3. SFA measurements on untreated alumina surfaces: smooth, undamaged surfaces (curve a); and rough, damaged surfaces after continuous sliding (curve b). Smooth surfaces coated with a monolayer of octadecyl phosphonic acid (curve c) slide with a higher friction at low loads than untreated alumina but remain undamaged even after prolonged sliding, keeping the friction substantially lower than rough surfaces at high loads. Experimental conditions: sliding velocity V = 0.05−0.5 μm/s, undeformed surface radii $R \approx$ 1 cm, temperature T = 25 °C, contact pressure range P = 1−10 MPa, relative humidity RH = 0% (curves a and c) and RH = 100% (curve b). Additional points measured on damaged alumina surfaces at RH = 0% also fell on curve b (not shown). Reprinted from Berman et al. *Tribol. Lett.* **1998**, *4*, 43−48, with permission from Kluwer Academic Publishers.

friction force is nonzero at zero load, but for even slightly damaged or roughened surfaces (curve b) F becomes directly proportional to L. From the changing shapes of the interference fringes, the damage was seen to consist of 3−5-nm-high asperities on the surfaces, which grew inward from the edges of the contact zone during continuous sliding until the whole contact area was uniformly rough. But the roughness remained "localized"; it did not appear to penetrate further *into* the surfaces or spread *outward* beyond the contact zone.[60]

The measured values of the friction coefficients of smooth and rough alumina surfaces as measured by SFA (μ = 0.07 and 0.48, respectively, as shown in Figure 3) are consistent with literature values for smooth alumina surfaces sliding under low loads (μ = 0.08) and macroscopic, presumably rough, surfaces sliding in air (μ = 0.33−0.52), respectively.[1] This strongly suggests that, unless special care is taken, under normal engineering conditions alumina surfaces slide in the damaged state with contact occurring through nano-asperities or small wear particles.

In the alumina experiments shown in Figure 3, the sliding of *smooth*, undamaged surfaces was *adhesion-controlled*: the real area A is well-defined and well-described by the JKR equation, $F \propto A$ at low loads, and F is finite at L = 0. In contrast, the sliding of *rough*, damaged surfaces was *load-controlled*: the "real" area of contact A is undefined, $F \propto L$, and $F \approx 0$ at L = 0. Thus, the introduction of surface roughness and wear particles results in the effective elimination of the adhesion and, as a consequence, a major reduction in the friction force at low loads (since adhesive contact now occurs only between micro- or nano-asperities) but a significant increase in the friction force at high loads (since F is now proportional to L rather than A, which has a weaker dependence on L).

The monolayer-coated alumina surfaces exhibited adhesion-controlled friction and were undamaged even after prolonged sliding at high loads corresponding to contact pressures of up to 10 MPa. In addition to providing a physical barrier against wear, the hydrophobic monolayers repel humidity and thus

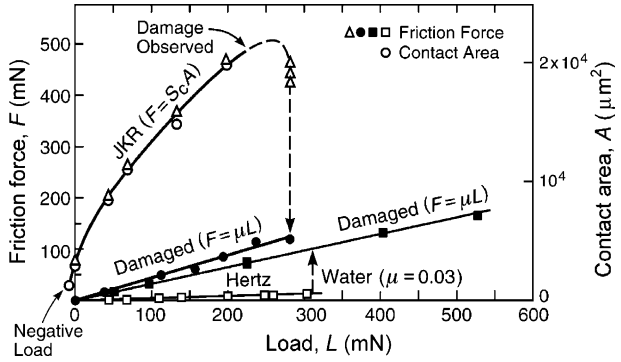

Figure 4. Friction force F and measured "real" contact area A vs load L for two undamaged mica surfaces sliding in adhesive contact in dry air (△, ○). The area A between these molecularly smooth surfaces is well described by the JKR theory even during sliding, and F is found to be directly proportional to A (○). The vertical dashed line and downward-pointing arrow show the transition from interfacial (wearless) friction to friction with wear (●). The sliding velocity was 0.2 μm/s. The two lowest curves show two mica surfaces sliding past each other while immersed in a 0.01 M KCl solution (nonadhesive conditions). The water film is molecularly thin, $D = 0.25-0.5$ nm, and the interfacial friction force is very low for smooth, undamaged surfaces (□). After the surfaces have become damaged, shown by the vertical arrow (■), the friction coefficient is ~0.3, which is similar to that for damaged surfaces in air (●). Adapted from Homola et al., 1989, 1990, with permission from ASME publishers.

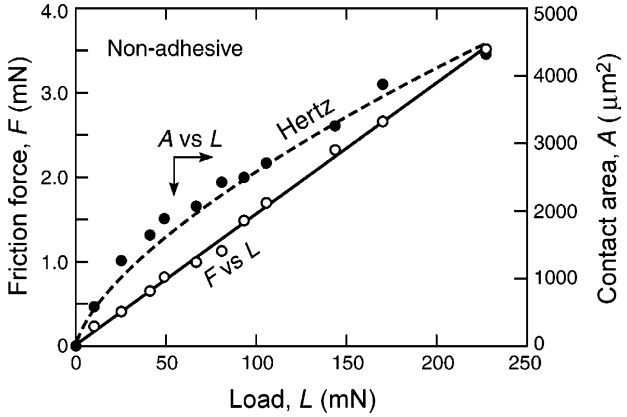

Figure 5. Measured friction force F (○) and real contact area A (●) as a function of load L between two molecularly smooth mica surfaces sliding in 0.5 M KCl solution at $T = 22$ °C where the intersurface forces are short ranged and repulsive (providing a nonadhering system). The sliding velocity was $V = 0.12$ μm/s. The dashed curve through the data points for A vs L (●) is the theoretical fit to the Hertz equation, using the measured undeformed radius of the surfaces $R = 0.95$ cm and $K = 4.0 \times 10^{10}$ N/m^2 for the effective elastic modulus of the substrate materials. Figure adapted from Berman et al. *Trib. Lett.* **1998**, *4*, 95−101, reprinted with permission from Kluwer Academic Publishers.

protect the alumina substrates from embrittlement and chemical attack by water.

The friction of adhesive and nonadhesive systems before and after damage are further compared in Figure 4. The top curve shows SFA results on both the friction forces and the "real" contact area of smooth, bare (untreated) mica surfaces in dry air where there is strong adhesion. This system shows an area-dependent friction with a high finite F at $L = 0$ and even at negative loads. However, as soon as the surfaces become damaged, F becomes linearly dependent on L ($\mu = 0.33$) and goes to zero at $L = 0$.[61] The high adhesive friction of the undamaged surfaces arises from a thin boundary film of organics and water that adsorb from the air and act as a poor boundary lubricant (but give a much lower friction force than for bare mica surfaces in an ultrahigh vacuum).[61] This adsorbed layer is displaced in aqueous salt solution, which dramatically improves the lubricity of smooth surfaces (lowest curve in Figure 4). The introduction of salt solution also replaces the strong adhesion between the surfaces with a short-range (1−2 nm) monotonically repulsive hydration force with a superimposed oscillatory component. The sliding conditions are therefore significantly changed, and a linear dependence of F on L is observed with a purely "load-controlled" friction coefficient of 0.02−0.03.[62]

In contrast to the localized damage that occurs on brittle surfaces such as alumina and silica, the damage of layered materials such as mica rapidly progresses across and beyond the contact zone as well as deep into the surfaces via delamination. The buildup of debris between the shearing surfaces eventually forces them apart by 0.1−1 μm. Once such large damage occurs, it does not seem to matter whether the original smooth surfaces were in air or in water or untreated or treated. Thus, in both cases shown in Figure 4, damage of the mica surfaces gave rise to a similar, load-controlled friction with similar friction coefficients of $\mu \approx 0.3$ both in air and in water (middle two curves). The formation of wear debris and "third bodies" separating the damaged surfaces precludes the measurement or even definition of any meaningful contact area A for such systems.

The friction forces and contact areas as functions of load of smooth but nonadhesive mica surfaces were further investigated in Figure 5. The mica surfaces were immersed in a concentrated salt solution, a system that eliminates the adhesion and is close to the one shown by the open squares in Figure 4.[63] The applied pressures during sliding were in the range $P = 0-50$ MPa, and the surface separations were typically $D = 0.2-0.5$ nm (lower values at higher loads), corresponding to one or two molecular layers of water between the sliding surfaces. The results show that, over a large range of loads, F varies linearly with L (open circles) but not with the molecular contact area A. The friction coefficient was 0.015−0.02 in agreement with the earlier results.[62] We note that this linearity was observed to hold even as the thickness D of the confined liquid film was changing with the load. For this nonadhesive case, the contact area is well described by Hertz theory, whereas for adhesive mica surfaces, it is well described by the JKR theory (Figure 4, open circles).

A linear dependence of F on L has also been observed for mica surfaces separated by hydrocarbon liquids.[64] Figure 6 shows the kinetic friction forces measured at high velocities across thin films of squalane, a branched hydrocarbon liquid ($C_{30}H_{62}$), which is also a model for lubricating oils. No adhesive forces are measured between mica surfaces across this liquid.[65] In general, as previously measured for squalane films at lower loads and room temperature, the film thickness decreased monotonically with increasing load. In the experiments of Figure 6, the thickness D varied monotonically from $D = 2.5$ to 1.7 nm as the load increased from $L = 0$ to 10 mN. The contact area is well described by Hertz theory, and the friction force increases linearly with load. In addition, the friction force at a given load, but not the contact area, was found to be velocity-dependent.

In an ultrahigh vacuum, certain materials can be brought into contact without a contaminant film between them, and the adhesion between two such surfaces, if smooth, can be quite high. Under such conditions, one can study the unlubricated (dry) sliding of two bare, strongly adhering surfaces. The friction

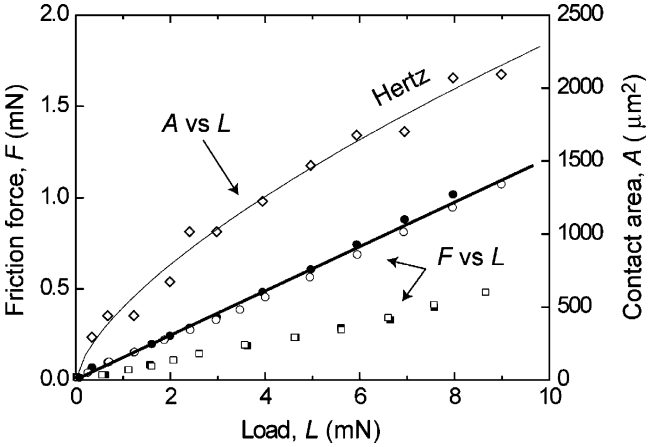

Figure 6. Steady-state friction forces F (●,○,■,□) and contact areas A (◇) vs load L measured with the SFA on a confined squalane film between two undamaged mica surfaces at two different velocities in the smooth (non stick-slip) sliding regime. Open symbols (○,□) show friction force data obtained on loading (increasing L); filled symbols (●,■) show unloading, all four of which are straight lines passing through the origin, one of which is shown by the thick line passing through the (○,●) points. The thin line is a fit of the Hertz equation to the A vs L data (◇) using $K = 1 \times 10^{10}$ N/m^2, $R = 2$ cm. The thickness D varies monotonically from $D = 2.5$ to 1.7 nm as the load increases from $L = 0$ to 10 mN. Adapted from Gourdon and Israelachvili, *Phys. Rev. E* **2003**, *68*, 021602/1−10. Copyright 2003 American Physical Society.

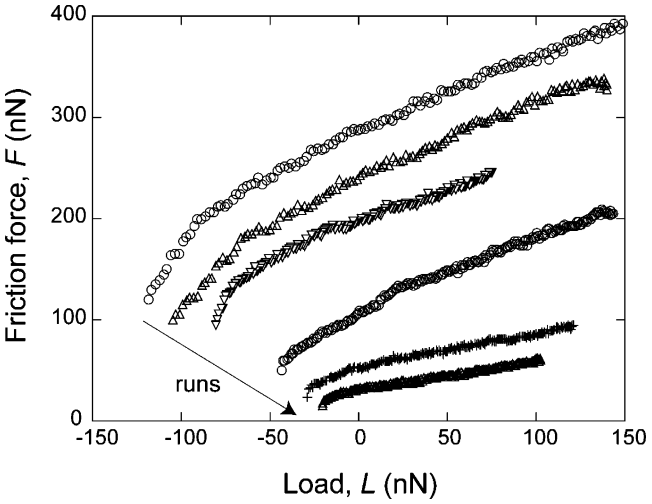

Figure 7. Scanning-induced reduction of adhesion and friction forces in FFM measurements with a Pt-coated tip in contact with a mica surface in UHV. After each run, the pull-off force also decreased in magnitude (not shown), implying a scanning-induced decrease in the adhesion energy from an initial value of $\gamma = 404$ mJ/m^2 on the first scan (not shown) to $\gamma = 19$ mJ/m^2 on the last scan (lowest curve) that paralleled the decrease in F shown here. The sliding in this system proceeded by stick-slip with a periodicity of the atomic spacing, and the friction force shown is the average "critical" or "static" friction force necessary to induce the slips. Reproduced with permission from Carpick et al. *Langmuir* **1996**, *12*, 3334−3340. Copyright 1996 American Chemical Society.

force between a platinum-coated AFM tip and a bare mica surface[53] (Figure 7) was found to be proportional to the contact area as predicted by the JKR theory.[28] But after repeated sliding over the same area, the adhesion decreased by more than 1 order of magnitude as did the friction force, and the curves appear to converge toward a straight line passing through the origin with a slope (friction coefficient) of $\mu \approx 0.3$. The decreased adhesion and friction was attributed to either structural or chemical changes at the interface between the tip and the mica, while wear of the mica surface or complete removal of the platinum coating could be excluded.[53]

Recent Theoretical and Conceptual Developments. *MD Simulations.* The MD simulations used in this study involved numerical integration of the equations of motion employing a simulation cell of lengths H_x, H_y, and H_z along the Cartesian coordinate axes. The cell contains both liquid molecules (the lubricant) and solid blocks (the surfaces), with periodic boundary conditions replicating the entire simulation cell in the two directions (x and y) parallel to the surfaces. The distance separating the two surfaces in the z direction defines the gap width D. In our simulations, the solid surfaces were modeled as flat gold (111) planes or as rough gold surfaces (see below). In the x and y directions, the solid blocks extend throughout the whole simulation cell, and in simulations of shear motion the two solids are translated in opposite directions to each other along the y axis. In the current study, the lengths of the solid blocks in the x and y directions were 200 Å for the flat surface confinement and 196 Å and 204 Å, respectively, for the rough confinement. The gap is filled with liquid *n*-hexadecane molecules (the simulated bulk lubricant is a liquid[66] at 298 K), and a typical simulation involved 600 molecules. In simulations of a particular system, the number of molecules does not vary for different applied normal loads and during shear motion.

Inside the gap, i.e., between the two solid surfaces, the alkane molecules are confined as a thin film with an average thickness D ranging in the present study between ∼8 and ∼11 Å. The hexadecane molecules were treated dynamically, while in most of the simulations, the gold atoms of the solid substrates were kept in their relaxed equilibrium positions. For the case of hexadecane molecules interacting with their full interaction potential with the gold surfaces (that is, including adhesive interactions between the lubricant molecules and the confining solid surfaces), we have verified that the results are essentially insensitive to the dynamics of the gold atoms. The hexadecane molecules are represented by the united-atom model, without rigid constraints; the interaction potentials include bond-bending, dihedral angle hindered rotations, and nonbonding intramolecular and intermolecular interactions. These molecular interaction potentials, as well as the 6−12 Lennard-Jones (LJ) interactions between the molecular segments and the gold atoms, have been described by us previously.[67] Many-atom embedded-atom potentials were employed in simulations where the gold surface atoms were treated dynamically.[68] We also remark that, in order to model the systems with *nonadhesive* interactions between the lubricant and solid surfaces, the *attractive* portion of the LJ potential between the wall atoms and the fluid molecules was removed.[69]

In these MD simulations, the phase-space trajectories of the system were generated through solutions of the atomistic equations of motion using the Verlet algorithm[70] and a numerical integration time step of 3 fs, with the temperature of the system controlled via the method described by Berendsen et al.;[71] the temperatures in the simulations were taken as either 300 or 350 K as indicated, which allowed the systems to equilibrate in a reasonable amount of computing time (in most of the analysis discussed below we treated data recorded in MD simulations performed at 300 K).

Preparation and Characterization of Rough Surfaces. To prepare atomically rough surfaces, we developed previously[72] the following procedure: (i) First, an equilibrated (at 350 K) solid gold slab (replicated in the x and y directions through the use of periodic boundary conditions) made of eight crystalline layers treated dynamically, and two additional bottom static

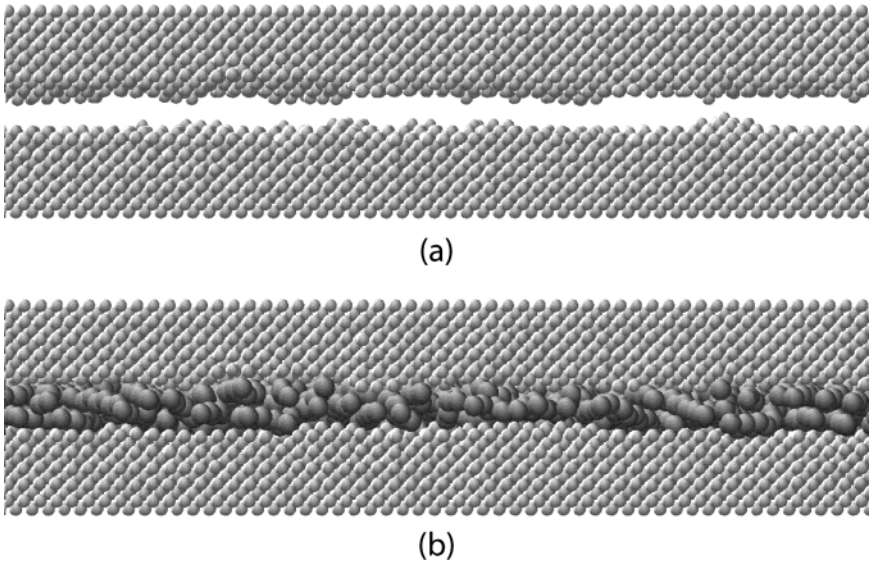

Figure 8. Rough gold surfaces separated by (a) vacuum and (b) hexadecane molecules.

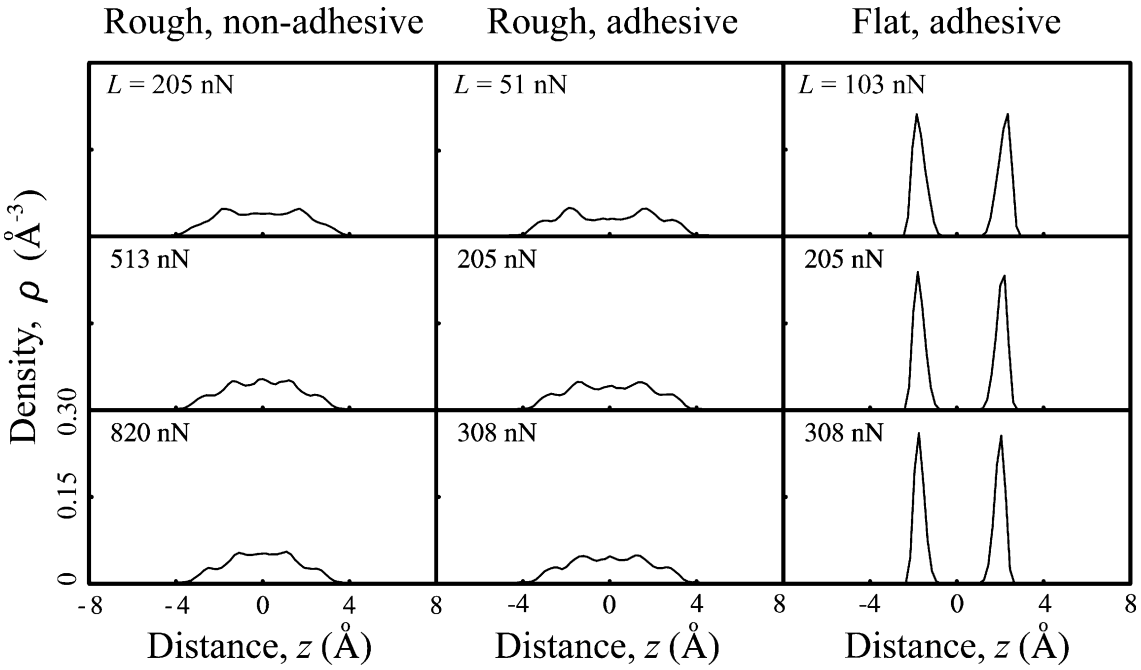

Figure 9. Hexadecane segmental density profiles, plotted as a function of distance along the axis normal to the solid planes (z) for selected values of the applied normal load. The left panel corresponds to the case of nonadhesive rough surfaces. The middle and right panels correspond, respectively, to adhesive rough and adhesive flat surfaces.

layers stacked as a face-centered-cubic crystalline solid and exposing the (110) surface, was heated to a temperature of 1100 K, resulting in melting of the top few layers of the solid. (ii) After equilibration of the system at 1100 K, it was rapidly cooled (quenched) to 350 K in 200 ps and then equilibrated at 350 K for an additional period of 300 ps. This procedure was applied separately to both the top and bottom confining slabs in order to create two uncorrelated rough surfaces.

Side views of the rough surfaces obtained through the preparation procedure described above are shown in Figure 8, with an empty gap in Figure 8a and a thin slice through the fluid-filled gap in Figure 8b. It is important to note that the topography of these *randomly* rough surfaces differs from the periodically ordered corrugations of atomically flat crystalline surfaces. The degree of effective roughness of the surfaces has been quantified by using the recorded height values (z), determined as described in ref 72, for evaluation of the lateral height−height correlation function $C(R) = \langle z(R)z(0)\rangle$, which correlates the surface heights (measured from a reference plane) between a site taken as the origin at (0,0) and a site at $R = (x_i,y_i)$. The angular brackets denote an average over the origins of R on the x_i-y_i grid, and R (<100 Å) is less than half the length of the confining solid surfaces in the x and y directions. From an exponential fit of e^{-R/l_c} to $C(R)$, we obtained a correlation length of $l_c = 6.9$ Å, which characterizes the roughness of the surfaces created by the procedure described above as short ranged; we also note that flat regions extending more than several atoms in size are rarely found on these rough surfaces. The root-mean-square deviation of the heights for each of the rough surfaces is 1.1 Å and that of the gap-width is about 1.6 Å.

Profiles of the density of the liquid lubricant recorded in equilibrium ($T = 350$ K) at several external loads for the lubricant confined by the rough surfaces and flat Au(111)

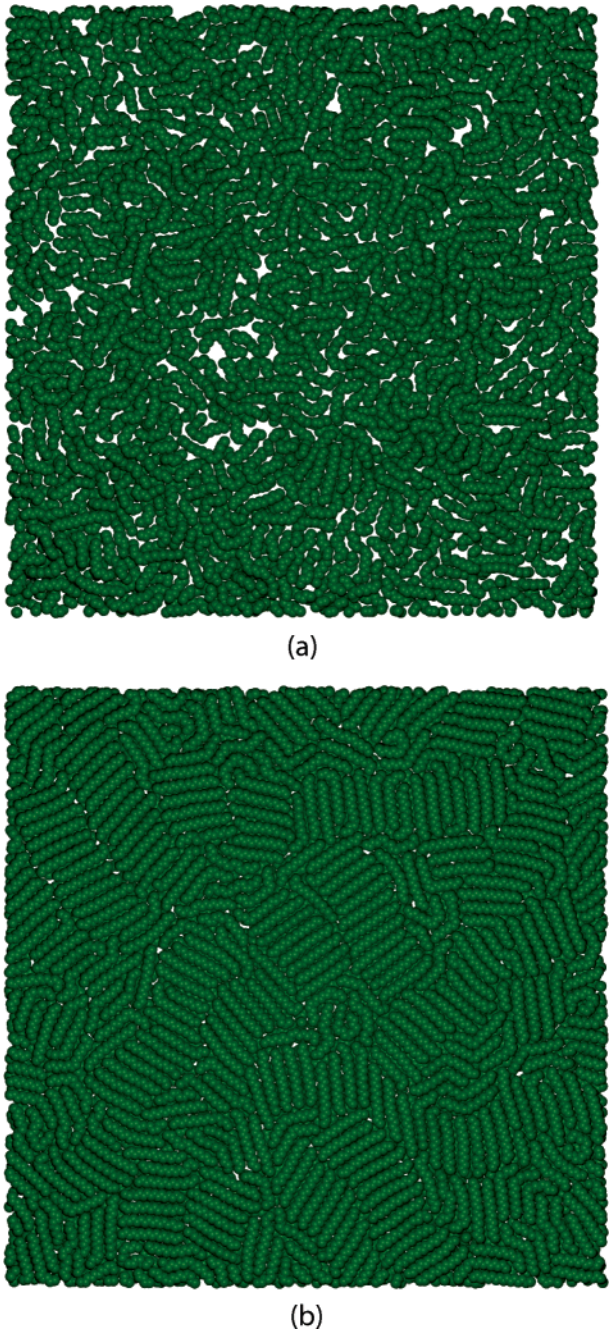

Figure 10. Top view of molecular arrangement in the interfacial region in contact with the solid surface. The top panel corresponds to the rough surface junction, and the bottom panel shows ordered domains corresponding to the flat surface junction. In both cases, the results are for adhesive interaction between the hexadecane molecules and the gold atoms.

surfaces with adhesive interaction between the hexadecane molecules and the metal atoms are displayed, respectively, in the middle and right panels of Figure 9. Comparison of these profiles shows formation of well-defined layers of the lubricant in the flat surface case and an essentially uniform distribution of the molecular segments in the gap between the rough surfaces. The density profiles for the case of rough confining surfaces with nonadhesive interactions between the surface atoms and the lubricant molecules show (see left panel in Figure 9) similar behavior to that exhibited in the adhesive rough surface case (middle panel in Figure 9).

In the case of the junction with flat Au(111) confining surfaces, the aforementioned formation of well-defined layers

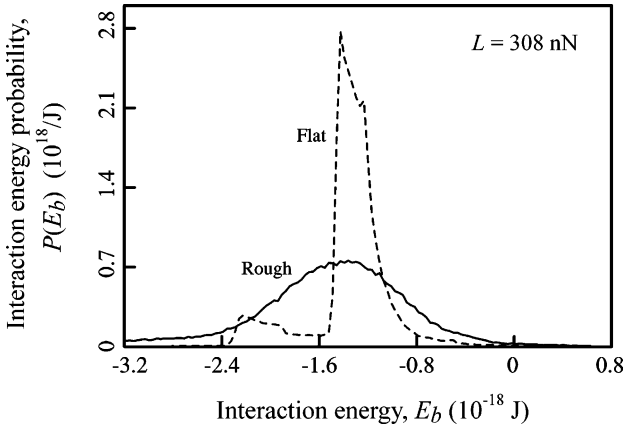

Figure 11. Distribution of the interaction energies (E_b) between the hexadecane molecular segments and the adhesive gold surfaces, calculated for a normal applied load $L = 308$ nN. The solid and dashed lines correspond to the rough and flat surfaces, respectively.

is accompanied by a high degree of intralayer order, characterized by domains composed of hexadecane molecules all lying in the plane of the surface, with the molecules in each domain being oriented parallel to each other (see Figure 10, bottom panel). In contrast, for the case of rough confining surfaces (adhesive or nonadhesive), neither layering normal to the (nominal) surface plane nor intermolecular orientational ordering occur (see Figure 10, top panel).

The structural heterogeneity of the confining surfaces is portrayed in the distribution of interaction energies between the alkyl (as well as end CH_3) segments of the hexadecane molecules and the surface atoms, with the one corresponding to the flat Au(111) being rather sharply peaked (see dashed line in Figure 11), while the energies corresponding to the rough confinement are distributed broadly (see solid line in Figure 11). As discussed by us elsewhere,[72] the energetic heterogeneity of rough-surface confinements in adhesive lubricated junctions prevents interfacial shear slip at the solid-liquid interfaces. In that work, it was argued that interfacial shear slip is inhibited under the above conditions by the inability of different regions of the confined interfacial liquid to respond collectively (and coherently) to the stress applied by the sliding solid surface.

Direct Analysis of the MD Simulations. By use of the methodology described in the previous two sections, simulations were performed for systems where the interaction between the alkane molecules and the confining surfaces are either nonadhesive or adhesive. Results for the total friction forces F (that is the force required in order to maintain a constant sliding velocity) as a function of the total applied load L for the two systems with rough confining surfaces are displayed in Figures 12 and 13, respectively. In both cases, the relative sliding velocity between the confining surfaces is $V = 1$ m/s. For the nonadhesive system, we also performed a series of simulations at a load of $L = 615$ nN and 300 K and found an almost constant friction force (of about $F = 54$ nN) in the range $V = 0.2-5.0$ m/s, with a small decrease in F below 0.5 m/s, falling by about 9 nN at $V = 0.2$ m/s, as shown in Figure 14. Similar nearly velocity-independent friction forces are often observed between boundary-lubricated (monolayer-coated) surfaces, exhibiting a similar drop in F at low V.[55]

For both the nonadhesive and adhesive cases, a linear relationship is found between the friction force and the applied load, except at the lowest loads, with a friction coefficient at 350 K of $\mu = 0.096$ for the nonadhesive system (Figure 12) and $\mu = 0.14$ or 40% higher for the adhesive one (Figure 13).

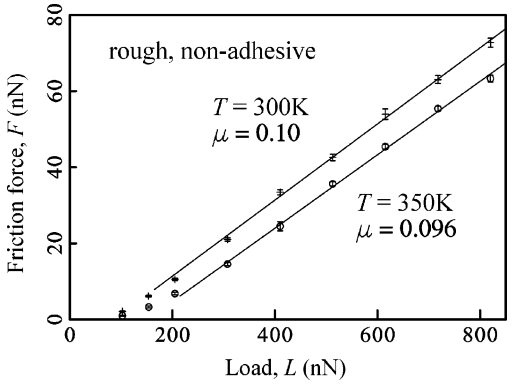

Figure 12. Total "macroscopic" friction force, F, plotted as a function of the total normal load, L, for rough nonadhesive surfaces lubricated by hexadecane molecules as shown in Figure 8b. For both temperatures, $T = 300$ and 350 K, the sliding velocity is $V = 1.0$ m/s. The quoted friction coefficients μ are defined by the *slopes* of the lines.

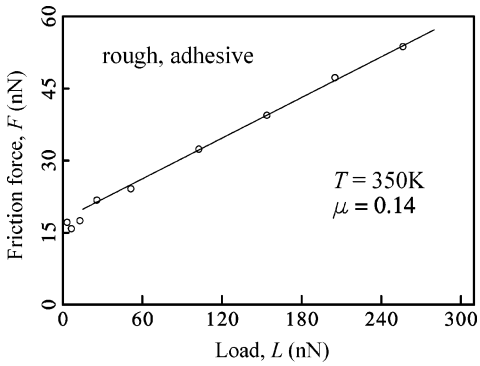

Figure 13. Similar to Figure 12 but for rough adhesive surfaces.

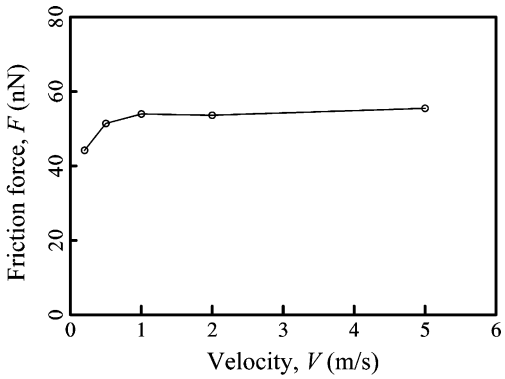

Figure 14. Dependence of the friction force on the sliding velocity, obtained from MD simulations of a hexadecane film lubricating the junction between nonadhesive rough surfaces at 300 K, under a load of 615 nN.

We also note that at the lower temperature of 300 K the nonadhesive friction coefficient is unchanged but that the absolute values of the friction forces are larger; i.e., a higher energy is spent to maintain a prescribed sliding velocity.

In the case of the nonadhesive system, we observe that the line describing the linear relation between the friction force and the load does not extrapolate back to the origin but curves toward $F = 0$ as $L \rightarrow 0$ due to wall slip at low loads (Figure 12). This type of limiting behavior was previously shown[73−75] to be due to the repulsive force−distance function between the "nonadhering" surfaces, which results in a viscous limit where the trapped film remains of finite thickness and behaves like a Newtonian liquid as $L \rightarrow 0$. In contrast, for the adhesive system (Figure 13), there is a finite friction force even for zero load,

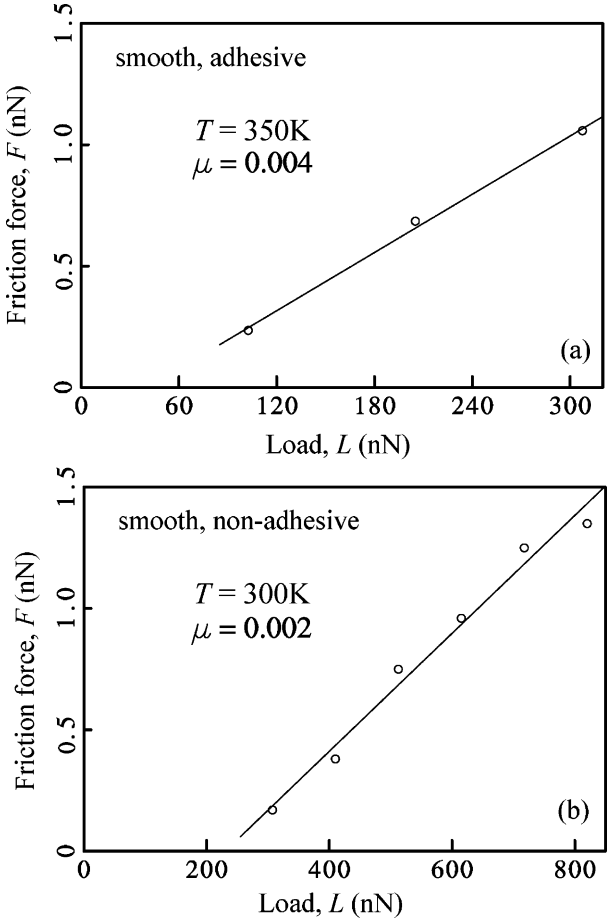

Figure 15. Similar to Figure 12 but for atomically smooth (crystalline) surfaces. Results for an adhesive junction are shown in (a), and those for a nonadhesive junction are shown in (b).

indicative of JKR behavior.[28] Similar results (not shown here) were obtained when the surface gold atoms were treated dynamically instead of statically. From these results, we conclude that the dynamics of the surface gold atoms does not influence the results of our simulations, and consequently, we have not considered these degrees of freedom in the rest of our simulations.

In contrast to the rough surfaces shown so far, we show in Figure 15 the results of simulations for sliding of two *atomically flat* crystalline (111) surfaces of gold lubricated by a thin hexadecane film. The results for an adhesive junction are shown in panel (a), and for a nonadhesive one, the results are displayed in panel (b). We note the exceedingly small friction coefficients of $\mu = 0.004$ and 0.002, respectively. Here, wall slip occurs for all values of the load studied by us; furthermore, in the small load regime ($F < 50$ nN in Figure 15a and $F < 250$ nN in Figure 15b), an essentially vanishing friction force is found, as in the nonadhesive case of rough surfaces discussed above (see Figure 12). Such behavior (i.e., wall slip) appears to be characteristic of atomically smooth surfaces and is related to the ordering of the lubricant molecules between two such interfaces.[72]

Since the boundary conditions at the solid-liquid interface strongly influence the frictional response, we further explore the dynamical nature of the lubricant response to shear motion of the confining surfaces and particularly issues pertaining to the dependencies of the degree of wall slip on the structure of the solid surfaces and on the interactions between the lubricant molecules and the surface atoms. To this aim, we display in Figure 16 the time variation of the average displacement Δ of

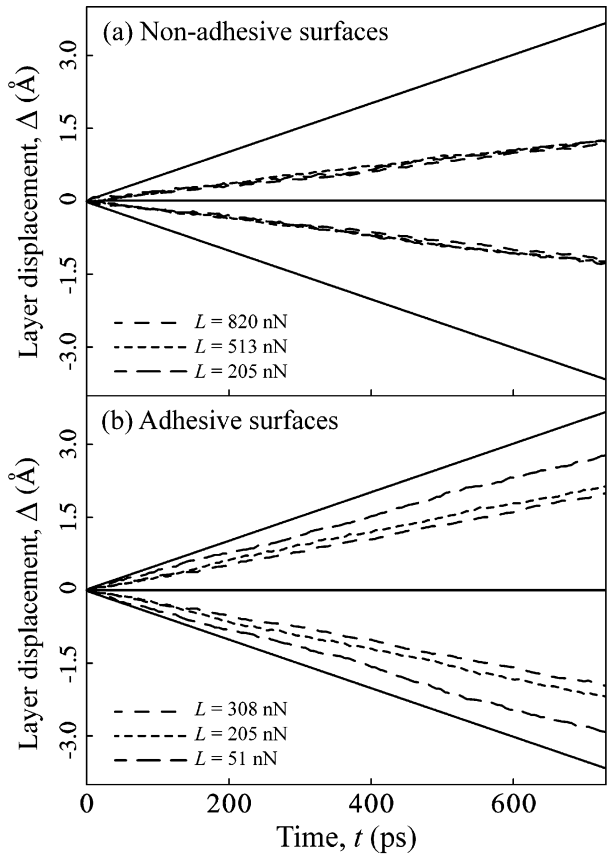

Figure 16. Average segmental displacements, Δ, for the two interfacial regions of the confined hexadecane film (one near the upper surface and the other near the bottom surface), plotted vs time during shear simulations of rough-surface junctions. Results are displayed (a) for the nonadhesive junction at the three indicated loads and (b) for the adhesive junction at three load values. The confining solid blocks move at a constant relative velocity of 1 m/s, and the solid straight lines correspond to the displacements of the top and bottom confining solid blocks which move in opposite directions.

molecular segments in the interfacial regions of the film, recorded for various values of the external load. These results were obtained through sliding simulations ($V = 1$ m/s at 350 K) for the nonadhesive (Figure 16a) and adhesive (Figure 16b) rough-surface junctions, respectively. The solid lines in this figure describe the displacement of the confining gold boundaries (translated at a constant velocity with respect to each other).

For the nonadhesive junction, pronounced wall slip is observed throughout the confined lubricant film for the entire range of load shown in the figure. This correlates with the weak coupling between the confining boundaries and the lubricant, resulting in weak momentum transfer between the two during sliding. The propensity for wall slip is seen to be smaller for the adhesive junction (Figure 16b), increasing as the load is increased. The weak wall slip (i.e., near-stick behavior) observed for the lowest load values reflects the aforementioned spatial and energetic heterogeneity of the interactions between the molecular segments and the surface atoms, which inhibits collective displacements involved with slip motion. As a result, in the small load regime sliding occurs in the interior of the lubricant film and not at the film-solid interface. On the other hand, for high loads, the resistance to sliding inside the film increases and a higher degree of wall slip emerges. We note here that, for the same velocity and temperature conditions and adhesive interactions, shear simulations of thin hexadecane films confined by flat crystalline surfaces (e.g., Au(111)) yield total wall slip for all load values as a consequence of the spatial homogeneity of the interaction energy between the molecules and the confining surfaces.

The direct analysis that we have applied above to the recorded MD results shown in Figures 12−16, yields information that will be treated in the following section as "theoretically generated empirical data"; we will refer to it as "macroscopic-level" data, since it corresponds to information obtained via averaging over the whole system (of length $\gg l_c$) and over the entire simulation time interval (typically, several nanoseconds, which is of the order of 10^6 integration time steps for each value of the externally applied load). To gain insights into the relationships between the molecular level frictional forces and those measured on the macroscopic scale, we perform in the following section a "local" analysis of the information recorded along the dynamical trajectories generated in the MD simulations. In this analysis, the nanoscale information (in space and time) is not coarse grained, thus maintaining molecular-level resolution, allowing exploration of various tribological relations, e.g., between the local (nanoscale) friction force and load, and how this relates to the macroscale dependencies, such as Amontons' equation.

Local-Load and Friction-Force Analysis. The local analysis that we describe below treats the results obtained from MD simulations performed, as described above, for specified values of the normal load, L, applied to the top solid surface (in this context, we regard this as the *macroscopic* load); the position of this surface varies dynamically so that the force on the surface arising from the confined molecule-wall interactions fluctuates about L. The top surface is binned into 6 Å × 6 Å square "tiles", each of which defines a "local" domain of the surfaces in which the instantaneous and time-averaged (local) normal and shear (friction) forces, l and f, are recorded (for each tile) at 6-ps intervals.[76] The 6-Å edge length of the tiles was chosen to approximate the height−height correlation length, l_c, characteristic of the rough surfaces (see the section about preparation and characterization of rough surfaces). The general nature of our results and conclusions do not change as long as the length scale of the tiles is small enough that it does not average out the effect of the surface roughness.

By computing such short time averages (of l and f) for a range of applied (macroscopic) normal loads, L, the statistical properties of the local forces and the manner in which they manifest themselves at the macroscopic scale could be explored. As a starting point, we compute for each value of the applied load L the probability density $P(l;L)$ for finding a local normal load with a value l. This is done in Figure 17a for the case of $n = 1025$ tiles within the lubricated rough nonadhesive junction. Additionally, we compute the local friction force f as a function of the local load l, shown in Figure 17b. The average value of the local friction force $\bar{f}$ may be expressed as

$$\bar{f}(L) = \int f(l;L)P(l;L)\,\mathrm{d}l \tag{5}$$

The corresponding average value of the local normal load $\bar{l}$ can be written as

$$\bar{l}(L) = \int lP(l;L)\,\mathrm{d}l \tag{6}$$

Figure 17a shows that the local normal force distribution is rather broad (recall that the highest applied total load used in the MD simulation when divided by the number of tiles n is about 0.8 nN), and that it exhibits a long tail. Significantly, the variation of the local friction force f as a function of the local normal force l is approximately parabolic for small loads (in

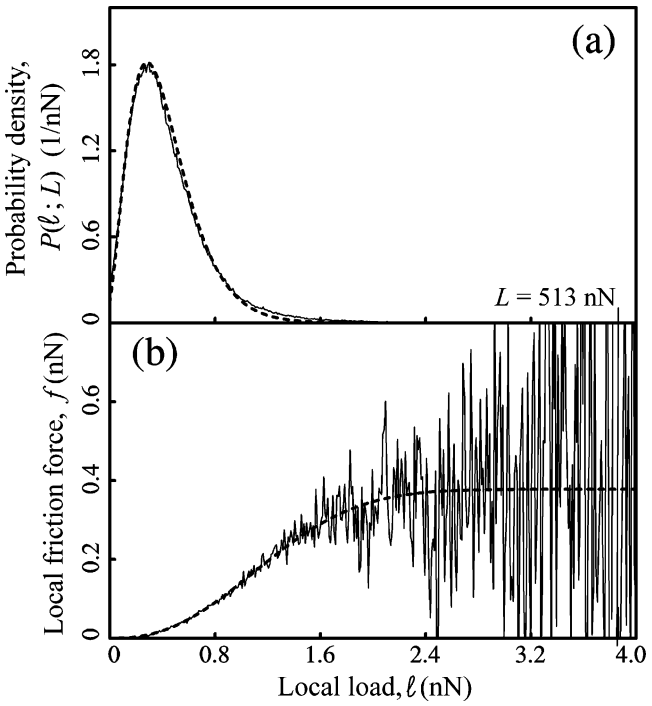

Figure 17. (a) Probability density $P(l)$ of the local normal load, l, for rough nonadhesive surfaces at a total normal applied load of $L = 513$ nN. The solid lines were recorded in MD simulations, and the dashed line is a gamma function fit to the data. The simulation was done at 300 K. (b) The local friction force f, as a function of the local normal load l. The dashed line is a fit to the data using the Weibull cumulative distribution function. The results for other values of the total applied load are of similar form as those shown here for the particular chosen normal load value.

particular, see Figure 17b for $l < 1$ nN); i.e., it is nonlinear and it *does not* obey Amontons' law. Similar results were obtained for all the other L values and also for *adhesive* rough-surface junctions (see below).

We now attempt to obtain an analytical description of the local quantities introduced in the above analysis and apply them first to the case of the rough-surface room-temperature nonadhesive junction. We have found that a shifted gamma distribution provides an adequate fit to the normal force local distributions up to the highest loads, at which point the exponential tail of the gamma distribution decays faster than the observed distribution (see Figure 17a). The gamma distribution may be expressed as[77]

$$p_g(x) = \frac{1}{b\Gamma(c)}\left(\frac{x-s}{b}\right)^{c-1}\exp\left(\frac{s-x}{b}\right) \qquad (7)$$

where s, b, and c are the shift, scale, and shape parameters. In our case $s = -0.054$ nN, $c = 3.5$, and $b(\bar{l}) = 0.018 + 0.26\bar{l}$, with b and $\bar{l}$ in units of nN.

The shape of the local friction force f plotted in Figure 17b vs the local normal force l, obtained from analysis of the MD data for a given value of L, has lead us to consider a particular probability distribution, namely, the Weibull distribution (WD). The WD originated as a tool for studies of the statistical distribution of the strengths of materials in which failure of the weakest component leads to complete failure of the material, and it is now used extensively in a wide range of fields where failure rates and lifetimes are important.[78] The WD function, $P_{WD}(x)$, defined below by eq 9, gives the fraction of samples that are expected to fail for stresses less than x. In our case, each of the "components" may be identified with a local region comprised, typically, of a small area of the surface (including its morphological heterogeneities) and the confined lubricant molecules, which are in a state of stress due to the relative motion of the confining boundaries. Sliding motion occurs when the molecular-scale free-energy barriers associated with the local regions are overcome. There is a spectrum of such activation barriers since both the surface morphologies and molecular conformations vary from one local region to another. The WD samples all of the molecular-scale barriers and associated barrier heights. With this identification, we may interpret $P_{WD}(l)$ as the *fraction of sliding barrier heights that are overcome for local normal loads that are smaller than l.* Accordingly, the local friction forces, $f(l)$ (i.e., the friction force averaged over all the local regions having a normal load l), are directly proportional to the fraction of surpassed barriers for sliding as given by the WD

$$f(l) = f(\infty)P_{WD}(l) \qquad (8)$$

where $f(\infty)$ is the local limiting friction force for large local loads (see Figures 17b and 19). The constant-velocity sliding mode of the solid surfaces in our simulations implies that all the barriers for sliding have been surpassed at any given time (although not simultaneously) and re-established as sliding proceeds. This is consistent with the above discussion pertaining to the relation between $f(l)$ and $P_{WD}(l)$ when we observe that *all* the sliding barriers can indeed be surmounted with the full spectrum of local loads found in the junction (which extends to large values of the local load).

The cumulative distribution function of the two-parameter WD (we find that a shift parameter is not necessary for describing our results) is given by

$$P_{WD}(x) = 1 - \exp[-(x/B)^m] \qquad (9)$$

Here, B is a scaling parameter, and m is often referred to as the Weibull modulus, or the Weibull exponent.

Returning to the local analysis of our MD results, we note that the plot of f vs l shown in Figure 17b has the appearance of a cumulative probability distribution, with high normal loads associated with a limiting value of the local friction force. In fact, the WD fits these curves extremely well for all the values of the applied loads used in the simulations. For example, using $f(\infty)P_{WD}(l)$ to fit the local friction force $f(l;L)$ calculated as described above for $L = 513$ nN, we obtain the fit shown by the dashed line in Figure 17b. The WD parameters used in our analysis of the nonadhesive junction were $f(\infty) = 0.378$ nN, $m = 2.4$, and $B(\bar{l}) = 0.85 + 1.11\bar{l}$, with B and $\bar{l}$ in units of nN. As a test of the quality of the analytical description of the local analysis, we use the above functional forms in eqs 5 and 6, and the results are shown in Figure 18 (points marked by stars). It is evident that our analysis predicts a highly linear relationship between the (temporally and spatially) *averaged* local friction force and the *averaged* local normal load.

The above local analysis was also applied to adhesive junctions (see Figures 13 and 15). Since for the case of a junction with flat crystalline surfaces the friction forces are exceedingly small for the range of sliding velocities used in our MD simulations, we focused on junctions of rough adhesive surfaces. The results of our analysis are shown in Figure 19, where a WD is again shown to fit the local friction forces (dashed line in Figure 19b), and the local normal force probability distribution is found to exhibit similar characteristics to that discussed above for rough nonadhesive junctions (compare the panels marked (a) in Figures 17 and 19).

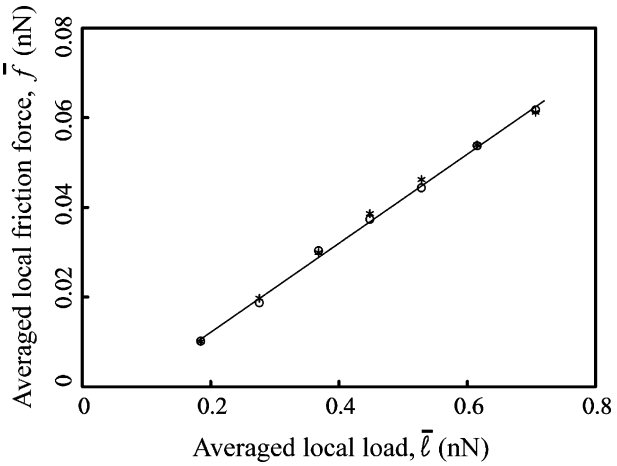

Figure 18. Averaged (spatially and temporally) local friction force $\bar{f}$ for nonadhesive rough surfaces plotted as a function of the average local normal load $\bar{l}$, calculated as described in the text. The circles are the simulation results. The stars are fits of the Weibull cumulative distribution function. The solid line gives a linear fit to the simulation results with a slope (friction coefficient) of 0.10.

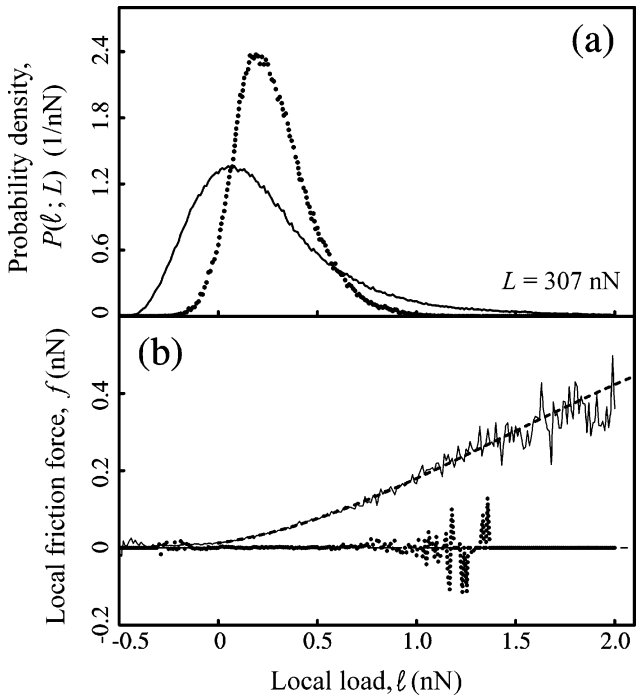

Figure 19. (a) The continuous curve shows the probability distribution of the local normal loads, $P(l)$, for rough adhesive surfaces with a total normal load of L = 307 nN. The dotted curve is the result of a simulation for adhesive atomically smooth crystalline gold (111) surfaces. (b) Simulation results of the local friction force, f, as a function of the local normal load, l. The dashed line corresponds to a fit to the data by a Weibull cumulative distribution function.

Figure 19 also shows our results for the flat crystalline adhesive junction (dotted curves in both panels), where we note that for this type of junction the local normal force probability distribution is comparatively narrower, with a much shorter tail, reflecting the fact that in the absence of morphological roughness the only remaining sources of heterogeneity that give rise to the broadening of the probability distribution function are the spatial and temporal variations of the conformations of the confined fluid molecules; for flat, but structured, crystalline surface junctions, these are limited by the ordering of the alkane molecules between the shearing surfaces.

3. Discussion and Conclusions

Comparison of Theory and Experiment. The focus of this article has been mainly on the origin of the coefficient of friction μ of nonadhering surfaces or junctions, where both theory (computer simulations) and experiment show that Amontons' law, eq 1a, $F = \mu L$, is surprisingly accurate. This 400-year-old law has had a number of previous continuum models,[3] all of which are model and system dependent, for example, depending on some chosen surface roughness, asperity deformations, and energy-dissipating mechanisms. And yet experiments have shown that eq 1 holds for very different systems and, even for the same system, the same friction coefficient is measured in SFA and AFM experiments where the length scales (e.g., junction size or slider-tip radius), contact areas, and pressures can differ by more than 6 orders of magnitude. The MD simulations presented here and in other recent work[72−75] show trends that correspond to, and are consistent with, experiments; specifically, the simulations predict a constant μ and yield values that are close to the observed ones. This correspondence is particularly significant in light of the different materials, systems, and conditions used in the experiments and in the theoretical simulations.[79] The picture that emerges from the analysis of the simulations presented in this paper is different from the earlier theories that are essentially "mechanical" rather than "thermodynamic". There is also good qualitative agreement for the more complex case of adhering surfaces, which we discuss below after we complete our analysis of nonadhering surfaces.

Tribological Ergodicity. For systems at thermodynamic equilibrium, such as a gas, a calculation of their mean properties requires that each molecule be allowed to sample the whole system. This means that a certain (strictly infinite) time is required if the averaging is to be thermodynamically or statistically correct. Alternatively, the averaging can be done over a finite time, but then a very large (again strictly infinite) number of molecules or "tiles" must be analyzed. This is the meaning of "ergodicity" for a system at equilibrium. The resulting properties, such as the mean velocity of the molecules, are generally extremely sharp and well defined, even as the local or instantaneous values vary widely in space and time.

For systems that are not at equilibrium, such as a tribological system, mechanical energy is continually being supplied to maintain a certain motion, which, in the steady state, is converted into heat at a fixed rate.[80] The MD simulations show that here, too, a kind of "dynamic" ergodicity applies; thus, when averaged over the whole (macroscopic) junction,[81] mechanical energy is converted to heat at a steady rate, but locally at any instant, the properties are far from the mean steady-state values. The MD simulations further suggest that the local compressions and expansions of the film molecules may be likened to miniature compression-decompression cycles that are only partially reversible. Essentially the same mechanism may be occurring for deformable asperities in the absence of a lubricating film (i.e., for dry contacts). This irreversibility determines the energy transferred and, ultimately, the friction force.[82] However, each asperity or surface segment (here referred to as a "tile") experiences a different instantaneous force, and if the tile is too small, its time-averaged friction force will be different from the system average. For example, a valley on a rough surface may never see an asperity of another surface and may therefore never experience a friction force. Its contribution to the overall friction will therefore be small or zero. In contrast, the top of an asperity may contribute well above the average. Thus, even in the steady state, the local tribological parameters fluctuate widely, are largely uncorrelated, and may not even average out

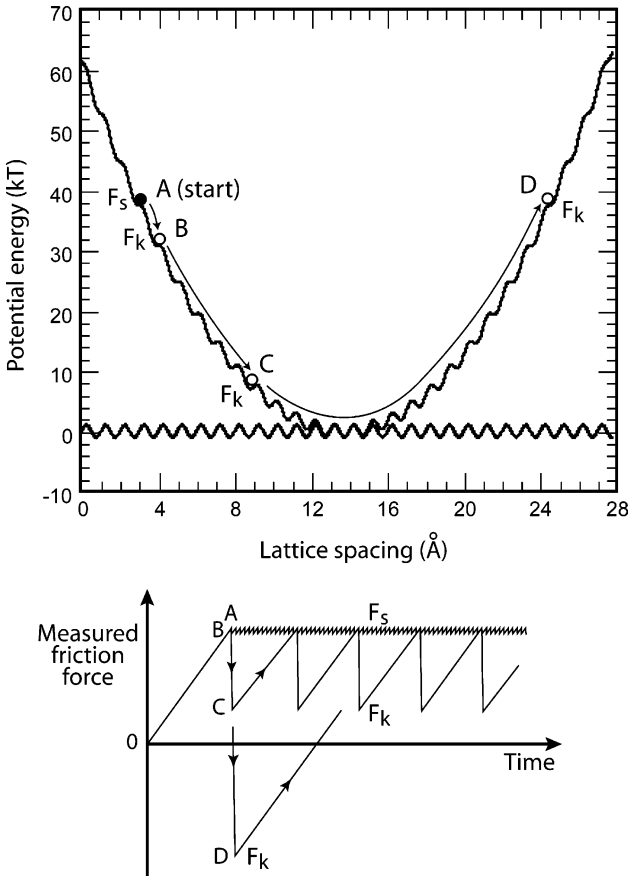

Figure 20. Simple schematic illustration of the most common molecular mechanism leading from smooth to stick-slip sliding in terms of the efficiency of the energy transfer from mechanical to kinetic to phonons. The potential energy of the corrugated surface lattice is shown by the horizontal sine wave. Let the depth of each minimum be ϵ, which is typically $>kT$. At equilibrium, a molecule will "sit" at one of these minima. When the molecule is connected to a horizontal spring, a smooth parabolic curve must be added to the horizontal curve. If this spring is now pushed or pulled laterally at a constant velocity V, the sine curve will move like a wave along the parabola carrying the molecule up with it (toward point A). When the point of inflection at A is reached, the molecule will drop and acquire a kinetic energy greater than ϵ even before it reaches the next lattice site. This energy can be "released" at the next lattice site (i.e., on the first collision), in which case the processes will now be repeated; each time the molecule reaches point A, it will fall to point B. The stick-slip here will have a magnitude of the lattice dimension and, except for AFM measurements that can detect such small atomic-scale jumps,[90,91] the measured macro- and microscopic friction forces (see bottom figure) will be smooth and independent of V. If the energy dissipation (or "transfer") mechanism is less than 100% efficient on each collision, the molecule will move further before it stops. In this case, the stick-slip amplitude can be large (point C) and the kinetic friction F_k can even be negative in the case of an overshoot (point D).

to the system average. However, for tiles above a certain dimension l_c or area l_c^2, their individual *time-averaged* values are the same as for other tiles, obeying Amontons' equation, and the same as for the macroscopic system. Similarly, for a large enough number of tiles, their instantaneous but *space-averaged* values are the same as those of the macroscopic system. The tribological system is thus ergodic-like, exhibiting well-defined average values, just like a gas, except that it is dynamic rather than at equilibrium.

An additional finding (conjectured here on the basis of most recent simulations),[83] and one that agrees with Amontons' law, is that, for nonadhering surfaces above a certain low load, the coefficient of friction is independent of the detailed nature of surface roughness that determines the critical tile dimensions l_c, even as each tile is topologically different from the next. In our MD simulations, l_c was small, less than 1 nm.

Origin of the Constancy of the Friction Coefficient. The apparent universality of the friction coefficient is not easy to explain even as both centuries-old experiments and, now, MD simulations show this to be the case. Again using the analogy of a gas, we seem to have a situation where many locally random or chaotic events give rise to a highly predictive phenomenon, exhibiting sharply defined properties (albeit with fluctuations in space and time which are again analogous to systems at equilibrium). Just as the Boltzmann distribution is a powerful tool for describing classical systems at equilibrium, the WD, eqs 8 and 9, serves a similar purpose for dynamic systems that involve a continuous making and breaking of multiple bonds. This distribution was found to properly account for the local forces and, when integrated, the constant friction coefficient predicted by the MD simulations. It is important to remark that the use of the WD is a matter of convenience; other probability distribution functions may also be applicable, with the requirement that they exhibit a long tail in order to predict Amontons-like behavior at the macroscopic scale.

The friction coefficient for nonadhering surfaces has often been attributed to the work done against the externally applied load by the "top" surface as its asperities climb over the asperities of the "bottom" surface. The mean asperity slope θ then gives the friction coefficient as $\mu = F/L = \tan\theta$. This is the basis of the Coulomb and Cobblestone models.[4,11,48] In contrast, the Bowden-Tabor and Greenwood-Williamson models consider the plastic or elastic deformations, respectively, of sheared asperities to derive Amontons' law.[14,15,18] With regard to molecular-level mechanisms of frictional processes, the MD simulations indicate that, while the above approaches may serve as useful phenomenological models, the spatial and temporal fluctuations revealed by the simulations are too large to be modeled in terms of semistatic macroscopic-like particles moving past each other.

Stick-Slip Friction. Our discussion has focused on smooth sliding. In many cases, sliding proceeds via stick-slip, which arises when the slope of the friction force-velocity curve is negative. In this regime (as opposed to the smooth-sliding regime), one cannot define a friction coefficient because the maxima and minima of the stick-slip spikes (often referred to as the static and kinetic friction forces, F_s and F_k, respectively) depend on the inertia (mass and stiffness) of the system or measuring apparatus. Figure 20 illustrates how stick-slip arises at the molecular level and how the magnitude of the spikes depends on the energy-dissipating processes between the molecules of the colliding surfaces. Stick-slip friction cannot be described by simple equations, and it requires a complex theoretical analysis (for example, involving rate-and-state equations, see, e.g., ref 84) and/or simulation,[43,48,84] which is outside the scope of this review.

Adhesion-Controlled and Load-Controlled Friction. Previous experiments have shown that in general the friction force can be split up into separate and additive (external) load-dependent and (internal) adhesion-dependent contributions. Thus, for nonadhering surfaces, the friction force is given by Amontons' law, $F = \mu L$, independently of the contact area A, while for adhering surfaces, there is an additional contribution that is proportional to the "real" molecular contact area (see Figure 21). This contribution exists at zero and even negative loads so long as the surfaces remain in contact over a finite area (see ref 48, Figure 9.17). Strictly speaking, however, the

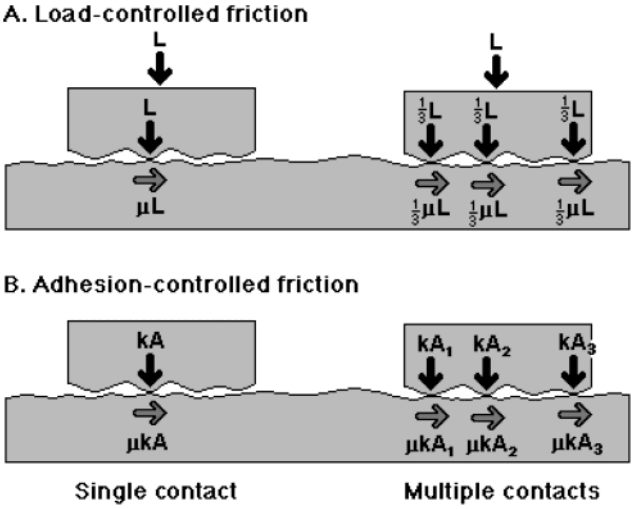

Figure 21. Difference in the local distribution of the external total applied load or normal adhesive force between load-controlled nonadhering surfaces (A) and adhesion-controlled surfaces (B). In the former case, the total friction force F is given either by $F = \mu L$ for one contact point (left side) or by $F = {}^1/_3\mu L + {}^1/_3\mu L + {}^1/_3\mu L = \mu L$ for three contact points (right side). Thus the load-controlled friction is always proportional to the applied load, independent of the number of contacts and of their geometry. In the case of adhering surfaces (B), the effective "internal" load is given by kA, where A is the real local contact area, which is proportional to the number of intermolecular bonds being made and broken across each single contact point. The total friction force is now given by $F = \mu kA$ for one contact point (left side), and $F = \mu kA_1 + \mu kA_2 + \mu kA_3) = \mu kA_{tot}$ for three contact points (right side). Thus, for adhesion-controlled friction, the friction is proportional to the real contact area, at least when no additional external load is applied to the system.

adhesion contribution is not proportional to the area but to the number of interatomic or intermolecular bonds that are broken and reformed when the surfaces slide laterally past each other.[63,85−87] The number of bonds is directly proportional to the contact area when the surfaces are perfectly smooth, when this area is referred to as the "real" contact area. For two perfectly flat, molecularly smooth surfaces, the "real" contact area is the same as the projected or "apparent" contact area. However, for rough surfaces, the real area of contact can be well below the apparent area (when the surfaces are hard) or well above it (when the surfaces are soft). These effects can give rise to adhesion and friction forces that can be orders of magnitude lower or higher than for molecularly smooth surfaces.[88]

Again, the phenomenological observation of a neat separation of the friction force into load-dependent and adhesion-dependent terms[48]

$$F = \mu L + \sigma A \tag{10}$$

is not borne out by the MD simulations, which do not show a simple separation between nonadhesive and adhesive contributions even though the overall F vs L curve (see Figure 13) is similar to the one expected to result from the assumption of two separate and additive contributions. However, as the simulations and eq 10 show, at very low loads ($L \rightarrow 0$), the second term begins to dominate even when it is small. For adhesive surfaces, this gives rise to a positive offset in the F vs L curve (cf. Figure 13), while for repulsive surfaces, it gives rise to a negative offset (cf. Figure 12 and refs 73−75). In the case of a liquid film trapped between the two surfaces, the shear stress σ is given by $\sigma =$ (viscosity)(sliding velocity)/(film thickness) where the film thickness will now also depend on the load L (this regime is commonly referred to as the hydrodynamic lubrication regime). Only for a hard-wall repulsion will the offset be (theoretically) zero. At the opposite extreme of very high loads, since $A \propto L^{2/3}$ for both JKR and Hertzian contacts, the first linear term in L eventually dominates even for adhesive systems, as observed experimentally.[48]

Meaning of the "Real", "Apparent", or "Projected" Contact Areas. The idea that the real contact area is an important or fundamental parameter that must be the starting point of any model of adhesion or friction has been the cause of much unnecessary confusion. Our MD analysis, which has been applied to both nonadhesive and adhesive junctions, does not involve the concept of an "area of contact" at any stage of the simulation. This may appear surprising, given that the area of contact (real or apparent) has always been a central parameter of models of friction. Likewise, the variation of the contact area with the applied load, as encapsulated in the Hertz and JKR theories (for nonadhering and adhering surfaces, respectively), has been central to models of adhesion, and both of these theories are commonly used to explain various tribological observations, including the linear dependence of the friction force on the applied load.

At the fundamental molecular level, the issue is simple; for clarity, let the intermolecular interactions are modeled in terms of some pair potential, such as the LJ potential $w(r) = 4\epsilon[(\sigma/r)^{12} - (\sigma/r)^6]$, where the atomic or molecular diameters are determined by the separation r at which the energy $w(r)$ is a minimum, e.g., $r_{min} = 2^{1/6}\sigma = 1.12\sigma$ and $w(r_{min}) = -\epsilon$ for the LJ potential. At the molecular level, the "contact area", e.g., between two atoms or molecules, is an undefined and unnecessary quantity. However, when calculating the interaction between two surfaces composed of molecules of known surface coverage (number density $\Gamma \approx 1/\sigma^2$ molecules/m^2), one may sum the interactions between all the molecules and then express the result in terms of an energy *per unit area*.[50] The "apparent" area of contact is therefore an acceptable parameter only when shear/slip occurs at a molecularly smooth interface where the number of interatomic or intermolecular bonds, contacts, or collisions per unit area is proportional to this area, in which case it can be associated with the "real" area. The apparent or projected area is therefore seen to be merely a convenient scaling parameter; the fundamental parameter is always the number or density of atoms, molecules, or bonds.[89] Even then, this density fluctuates enormously in both space (position) and time, this being one of the main messages of the article.

Acknowledgment. The theoretical work at the Georgia Institute of Technology was supported by the Department of Energy (DOE) under Grant DE-FG05-86ER45234, and the experimental work at University of California at Santa Barbara was supported by DOE Grant DE-FG03-87ER45331. Numerical simulations were performed in part at the DOE National Energy Research Supercomputing Center (NERSC) located in Berkeley, California. M.R. thanks the Academy of Finland (Grant 48879) for financial support. We also thank R. Carpick for providing us with the data of Figure 7.

References and Notes

(1) Blau, P. In *Friction, Lubrication, and Wear Technology, ASM Handbook*; Blau, P., Ed.; ASM International: Materials Park, 1992; Vol. 18, p 74.

(2) One may even think of these two forces as the lateral and normal components of some friction force function $F(\theta)$ where θ is the angle at which two bodies or surfaces are being moved relative to each other.

(3) Dowson, D. *History of Tribology*; Longman: London, 1979.

(4) Amontons, G. *Mémoires de l'Académie Royale A*; 1699, pp 257−282.
(5) Yoshizawa, H.; Chen, Y.-L.; Israelachvili, J. *J. Phys. Chem*. **1993**, *97*, 4128.
(6) Schwarz, U. D.; Bluhm, H.; Hölsher, H.; Allers, W.; Wiesendanger, R. In *Physics of sliding friction*; Persson, B. N. J., Tosatti, E., Eds.; Kluwer Academic: Dordrecht, 1996; pp 369−402.
(7) For example, a solid block of metal cannot be sheared except by a very high shear stress, yet this is an example of two smooth surfaces in adhesive contact under no external (normal) load.
(8) Rabinowicz, E. *Friction and Wear of Materials*, 2nd ed.; Wiley: New York, 1995.
(9) *Physics of sliding friction*; Persson, B. N. J., Tosatti, E., Eds.; Kluwer Academic: Dordrecht, 1996.
(10) Analogous to the fixed, nonfluctuating average velocity of the molecules in a gas even though at any instant any particular molecule may have almost any velocity.
(11) Coulomb, C. A. *Mém. Math. Phys. (Paris)* **1785**, 161.
(12) Euler, L. *Mém. Acad. Sci. (Berl.)* **1750**, *4*, 122.
(13) Leslie, L. *An Experimental Inquiry Into The Nature and Propagation of Heat*; Bell and Bradfute: Edinburgh, 1804.
(14) Bowden F. P.; Tabor, D. *An Introduction to Tribology*; Anchor Press/Doubleday: Garden City, 1973.
(15) Bowden F. P.; Tabor, D. *Proc. R. Soc. London* **1939**, *A169*, 391.
(16) Hertz, H. *J. Reine Angew. Math*. **1881**, *92*, 156.
(17) Maugis, D.; Pollock, H. M. *Acta Metall*. **1984**, *32*, 1323.
(18) Greenwood, J. A.; Williamson, J. B. P. *Proc. R. Soc. London* **1966**, *A295*, 300.
(19) Greenwood, J. A. In *Fundamentals of Friction: Macroscopic and Microscopic Processes*; Singer, I. L., Pollock, H. M., Eds.; Kluwer: Dordrecht, 1992; pp 37−56.
(20) Kapoor, A.; Johnson, K. L. *Proc. R. Soc. London* **1994**, *A445*, 367.
(21) Fuller, K. N. G.; Tabor, D. *Proc. R. Soc. London* **1975**, *A345*, 327.
(22) Maugis, D. *J. Adhes. Sci. Technol*. **1996**, *10*, 161.
(23) Sayles R. S.; Thomas, T. R. *Nature* **1978**, *271*, 431.
(24) Majumdar, A.; Bhushan, B. *J. Tribol.* **1991**, *113*, 1.
(25) Greenwood, A.; Wu, J. J. *Meccanica* **2001**, *36*, 617.
(26) Derjaguin, B. V. *Z. Phys.* **1934**, *88*, 661.
(27) A number of scientists had previously suggested equations of this form, including Coulomb.
(28) Johnson, K. L.; Kendall, K.; Roberts, A. D. *Proc. R. Soc. London* **1971**, *A324*, 301.
(29) Binnig, G.; Quate, C. F.; Gerber, Ch. *Phys. Rev. Lett*. **1986**, *56*, 930.
(30) Tabor, D.; Winterton, R. *Proc. R. Soc. London* **1969**, *A312*, 435
(31) Israelachvili, J. N.; Tabor, D. *Proc. R. Soc. London* **1972**, *A331*, 19.
(32) Israelachvili, J. N.; Adams, G. E. *J. Chem. Soc., Faraday Trans.* **1978**, *I74*, 975.
(33) Bhushan, B.; Israelachvili, J. N.; Landman, U. *Nature* **1995**, *374*, 607.
(34) Leckband, D.; Israelachvili, J. N. *Quart. Rev. Biophys*. **2001**, *34*, 105.
(35) Granick, S. *Phys. Today* **1999**, 26.
(36) Klein, J.; Kumacheva, E. *Science* **1995**, *269*, 816.
(37) Carpick, R. W.; Salmeron, M. *Chem. Rev*. **1997**, *97*, 1163.
(38) Gnecco, E.; Bennewitz, R.; Gyalog, T.; Meyer E. *J. Phys.: Condens. Matter* **2001**, *13*, R619.
(39) Landman, U.; Luedtke, W. D.; Ribarsky, M. W. *J. Vac. Sci. Technol.* **1989**, *A7*, 2829.
(40) Landman, U.; Luedtke, W. D.; Nitzan, A. *Surf. Sci*. **1989**, *210*, L177.
(41) Landman, U.; Luedtke, W. D.; Burnham, N. A.; Colton, J. R. *Science* **1990**, *248*, 454.
(42) Landman, U.; Luedtke, W. D.; Ringer, E. M. In *Fundamentals of Friction: Macroscopic and Microscopic Processes*; Singer, I. L., Pollock, H. M., Eds.; Kluwer: Dordrecht, 1992; pp 463−510.
(43) Thompson, P. A.; Robbins M. O. *Science* **1990**, *250*, 792.
(44) Robbins, M. O.; Müser, M. H. In *Modern Tribology Handbook*; Bhushan, B., Ed.; CRC Press: Boca Raton, FL, **2001**; p 717.
(45) For recent simulations and modeling pertaining to Amontons' law in the static regime, see: Müser, M. H.; Wenning, L.; Robbins, M. O. *Phys. Rev. Lett*. **2001**, *86*, 1295.
(46) Also called lateral force microscope, an AFM with a lateral force-measuring capability.
(47) McGuiggan, P. M.; Zhang, J.; Hsu, S. M. *Tribol. Lett*. **2001**, *10*, 217.
(48) Israelachvili, J. N.; Berman, A. D. In *Handbook of Micro/Nanotribology* 2nd ed.; Bhushan, B., Ed.; CRC Press: Boca Raton, FL, 1999; pp 371−432.
(49) All surfaces adhere, however weakly, especially in air. In the original experiments by Leonardo, Amontons, and Coulomb, the surfaces were rough and hard so that true (adhesive) contact occurred only between a few asperities, and the resulting adhesion was far too small to have a significant or measurable effect on the friction force.
(50) Israelachvili, J. N. *Intermolecular and Surface Forces*, 2nd ed.; Academic Press: London, 1991.
(51) Ruths, M. *Langmuir* **2003**, *19*, 6788.
(52) Enachescu, M.; van den Oetelaar, R. J. A.; Carpick, R. W.; Ogletree, D. F.; Flipse, C. F. J.; Salmeron, M. *Tribol. Lett*. **1999**, *7*, 73.
(53) Carpick, R. W.; Agraït, N.; Ogletree, D. F.; Salmeron, M. *Langmuir* **1996**, *12*, 3334.
(54) Kim, H. I.; Houston, J. E. *J. Am. Chem. Soc*. **2000**, *112*, 12045.
(55) Ruths, M.; Alcantar, N. A.; Israelachvili, J. N. *J. Phys. Chem.* **2003**, *107*, 11149.
(56) Liu, G.-y.; Salmeron, M. B. *Langmuir* **1994**, *10*, 367.
(57) Lio, A.; Morant, C.; Ogletree, D. F.; Salmeron, M. *J. Phys. Chem. B* **1997**, *101*, 4767.
(58) We note that, while all the lengths and forces differ by many orders of magnitude, the sliding velocities used in the SFA and FFM studies were similar.
(59) Steinberg, S.; Ducker, W.; Vigil, G.; Hyukjin, C.; Frank, C.; Tseng, M. Z.; Clarke, D. R.; Israelachvili, J. N. *Science* **1993**, *260*, 656.
(60) Berman, A.; Steinberg, S.; Campbell, S.; Ulman, A.; Israelachvili, J. *Tribol. Lett.* **1998**, *4*, 43.
(61) Homola, A. M.; Israelachvili, J. N.; Gee, M. L.; McGuiggan, P. M. *J. Tribol.* **1989**, *111*, 675.
(62) Homola, A. M.; Israelachvili, J. N.; McGuiggan, P. M.; Lee, M. L. *Wear* **1990**, *136*, 65.
(63) Berman, A.; Drummond, C.; Israelachvili, J. *Tribol. Lett.* **1998**, *4*, 95.
(64) Gourdon, D.; Israelachvili, J. *Phys. Rev. E*. **2003**, *68*, 021602/1−10.
(65) Drummond, C.; Israelachvili, J. *Macromolecules* **2000**, *33*, 4910.
(66) Mondello, M.; Grest, G. S. *J. Chem. Phys.* **1997**, *106*, 9327.
(67) Gao, J.; Luedtke, W. D.; Landman, U. *J. Chem. Phys.* **1997**, *106*, 4309.
(68) Adams, J. B.; Foils, S. M.; Wolfer, W. G. *J. Mater. Res.* **1989**, *4*, 102.
(69) In general, adhesive and nonadhesive refer to the two surfaces interacting across the film between them, whether air or liquid. In other words, it refers to what one would measure when pulling the two surfaces apart. Thus, when separated by a liquid film, the film molecules and film-surface forces could be attractive (adhesive) while the surface-surface interaction is not. In our simulations, the direct interactions between the two surfaces is much smaller than the film-surface interactions, and thus adhesiveness, or nonadhesiveness, reflects directly the nature of the interactions between the molecular film and the confining surfaces.
(70) Verlet, L. *Phys. Rev*. **1967**, *159*, 98.
(71) Berendsen, H. J. C.; Postma, J. P. M.; Van Gunsteren, W. F.; Di Nola, A.; Haak, J. R. *J. Chem. Phys*. **1984**, *81*, 3684.
(72) Gao, J.; Luedtke, W. D.; Landman, U. *Tribol. Lett*. **2000**, *9*, 3.
(73) He, G.; Müser, M. H.; Robbins, M. O. *Science* **1999**, *284*, 1650.
(74) He, G.; Robbins, M. O. *Tribol. Lett.* **2001**, *10*, 7.
(75) He, G.; Robbins, M. O. *Phys. Rev. B* **2001**, *64*, 035413/1−13.
(76) We note here that the relative shear velocity between the two solid surfaces is 1 m/s = 0.01 Å/ps so that in a 6-ps interval the relative displacement of the surfaces is a mere 0.06 Å and the relative local geometry of the confining surfaces has hardly changed. Extending the time-averaging interval to larger values, e.g., 36 ps, has little or no effect on the calculated local averaged values.
(77) Feller, W. *An Introduction to Probability Theory and Its Applications,*; 2nd ed.; Wiley: New York, 1971; Vol. 2.
(78) *Probabilistic Methods in the Mechanics of Solids and Structures*; Eggwertz, S., Lind, N. C., Eds.; Springer: Berlin, **1985**.
(79) We comment here on certain specific differences between the conditions employed experimentally and theoretically. (i) The sliding velocity used in the simulations is several orders of magnitude faster than in the experiments. Note, however, that friction forces commonly exhibit a weak dependence (logarithmic or weaker) on the sliding velocity. (ii) The contact used in the simulations is "nominally" flat, that is, a uniform normal stress is applied, while in the SFA experiments, the surfaces are originally curved, leading to a highly nonuniform stress distribution. While the details of this stress distribution may be expected to influence the results, SFA experiments with mica and boundary-lubricated mica surfaces clearly show that a single constant shear stress appears to describe the measured friction forces when these are in the low-load, adhesion-controlled regime, i.e., when $F \propto A$.
(80) The more commonly used expressions "energy dissipated" or "energy lost" are misleading since no energy is ever lost; it is only converted or transferred from one form to another or to a different location.
(81) Here the junction is the macroscopic system, composed of smaller segments or "tiles".
(82) By definition, the energy transferred (E) is equal to the product of

the friction force (F) and the displacement (x), i.e., $E = Fx$. The *rate* of energy transfer is therefore given by $dE/dt = F\,dx/dt = Fv$, where v is the sliding velocity.

(83) Gao, J.; Luedtke, W. D.; Landman, U. Unpublished results.

(84) Gao, J.; Luedtke, W. D.; Landman, U. *J. Phys. Chem. B* **1998** , *102*, 5033.

(85) Israelachvili, J. N.; Berman, A. *Isr. J. Chem*. **1995**, *35*, 85.

(86) Gao, J. et al. To be published.

(87) Vigil, G.; Xu, Z.; Steinberg, S.; Israelachvili, J. N. *J. Colloid Interface Sci*. **1994**, *165*, 367 (see Figure 21 on p 71).

(88) Israelachvili, J. N. In *Fundamentals of Tribology − Bridging the gap between the macro-, micro- and nanoscales*, NATO Advanced Science Institute Series; Bhushan, B., Ed.; Kluwer Academic Publishers: Dordrecht, 2001; pp 631−650.

(89) The number density can be per unit area (m^{-2}) or volume (m^{-3}), depending on the situation.

(90) Mate, C. M.; McClelland, G. M.; Erlandsson, R.; Chiang, S. *Phys. Rev. Lett.* **1987**, *59*, 1942.

(91) Landman, U.; Luedtke, W. D.; Nitzan, A. *Surf. Sci.* **1989**, *210*, L177.